TEKTONIKA

The Pınarbaşı Metamorphic Sole (Turkey) as a Geological Archive of Subduction Initiation in the Cretaceous Neotethys Ocean

Kalijn Peters [1], Alexis Plunder [2,3], Carl Guilmette [4], Fraukje M. Brouwer [5], Klaudia F. Kuiper [5], Jan R. Wijbrans [5], Herman L. M. van Roermund[1], Roel van Elsas [5], Hidde Gerretsen[1], Jasper Hupkes [1], Marco Maffione [6], Douwe J. J. van Hinsbergen [*1]

[1]Department of Earth Sciences, Utrecht University, Utrecht, the Netherlands | [2]BRGM – French Geological Survey, F-45060 Orléans, France | [3]ISTO, UMR 7327, Université d'Orléans, CNRS, BRGM, F-45071 Orléans, France | [4]Département de Géologie et de Génie Géologique, Université Laval, Québec, QC, Canada | [5]Department of Earth Sciences, Vrije Universiteit Amsterdam, Amsterdam, the Netherlands | [6]School of Geography, Earth and Environmental Sciences, University of Birmingham, Birmingham, UK

Abstract Metamorphic soles are metamorphosed oceanic crustal and pelagic sedimentary rocks that underlie supra-subduction zone (SSZ) ophiolitic mantle. Soles record the juvenile plate interface history and SSZ ophiolites record the onset of upper plate extension. Despite their importance and widespread occurrence, few soles have been studied in detail, a notable exception being the Cretaceous Oman sole. Here, we describe the Cretaceous Pınarbaşı metamorphic sole that formed in Central Anatolia. We show that the 240 m thick sole has a 10 m thick high-temperature (HT) top with melt pockets that reached P–T conditions of 1.2–1.4 GPa and 775–825 °C, and a 230 m thick low-temperature (LT) amphibolite- and greenschist-facies base. $^{40}Ar/^{39}Ar$ hornblende ages reveal HT and LT sole cooling below ∼500 °C by 93–95 Ma, similar to, or slightly older than, nearby ophiolitic crustal ages. The Pınarbaşı section contains an HT slice interleaved in the LT base that records regional sole imbrication by subduction erosion during sole growth. The Pınarbaşı metamorphic sole is a lateral equivalent of the Oman sole and likely formed at the same nascent plate boundary. Slightly younger cooling and spreading ages at Pınarbaşı likely indicate lateral variations in subduction zone maturation and onset of upper plate extension. Their comparison constrains regional geodynamic drivers and plate kinematic context of subduction initiation.

Executive Editor:
J Kim Welford
Technical Editor:
Mohamed Gouiza

Reviewers:
Anonymous reviewer 1
Anonymous reviewer 2

Submitted:
10 December 2025
Accepted:
25 September 2026
Published:
17 November 2026

1 Introduction

The initiation of new subduction zones is a key ingredient of the plate tectonic cycle and so-called supra-subduction zone (SSZ) ophiolites (*Pearce et al.*, 1984; *Shervais*, 2001; *Stern and Bloomer*, 1992; *Stern et al.*, 2012), and their underlying metamorphic soles that formed at the initial subduction interface are recognized as the geological record of this process (*Agard et al.*, 2016; *Guilmette et al.*, 2018; *Hacker*, 1994; *Jamieson*, 1980; *Wakabayashi and Dilek*, 2003). SSZ ophiolites contain a magmatic crust that formed from shallow mantle melting in the forearc above a (nascent) subducting slab (*Stern and Bloomer*, 1992; *Stern et al.*, 2012) and form belts spanning 1000s of km-long paleo-plate boundaries (e.g., *Dilek and Furnes*, 2011; *Rioux et al.*, 2016). SSZ ophiolites are interpreted to reflect catastrophic slab sinking and upper plate extension that is well explained by sudden foundering of a subducting plate upon inception of slab pull in a young subduction zone (*Hall et al.*, 2003; *Kotowski et al.*, 2026; *Li and Gurnis*, 2024; *Stern*, 2004; *Stern and Gerya*, 2018). Direct constraints on how initial thrusting and subsequent collapse of the subduction zone occurred rely on the study of metamorphic soles (e.g., *Agard et al.*, 2016; *Guilmette et al.*, 2018, 2023; *Wakabayashi and Dilek*, 2003), of which a few key outcrops, in localities like Oman and Newfoundland, have become archetypal and dominate the current thinking.

Metamorphic soles comprise crustal, typically metabasaltic and metasedimentary rocks that are found underneath ophiolites, and that display high-temperature metamorphism. The archetypal Cambrian Bay of Islands metamorphic sole in Newfoundland (*Dewey and Casey*, 2013; *Fournier-Roy et al.*, 2024, 2026; *Jamieson*, 1980), and the Cretaceous Sema'il metamorphic sole of Oman (*Guilmette et al.*, 2018; *Hacker and Gnos*, 1997; *Searle and Cox*, 2002) display an up to ∼500 m thick series of metamorphic rocks with an inverted metamorphic gradient, from high-pressure granulite-facies rocks at the top to low-pressure greenschist-facies rocks at the base. Elements of those soles are recognized worldwide, irrespective of the tectonic setting in which subduction

*✉ d.j.j.vanhinsbergen@uu.nl

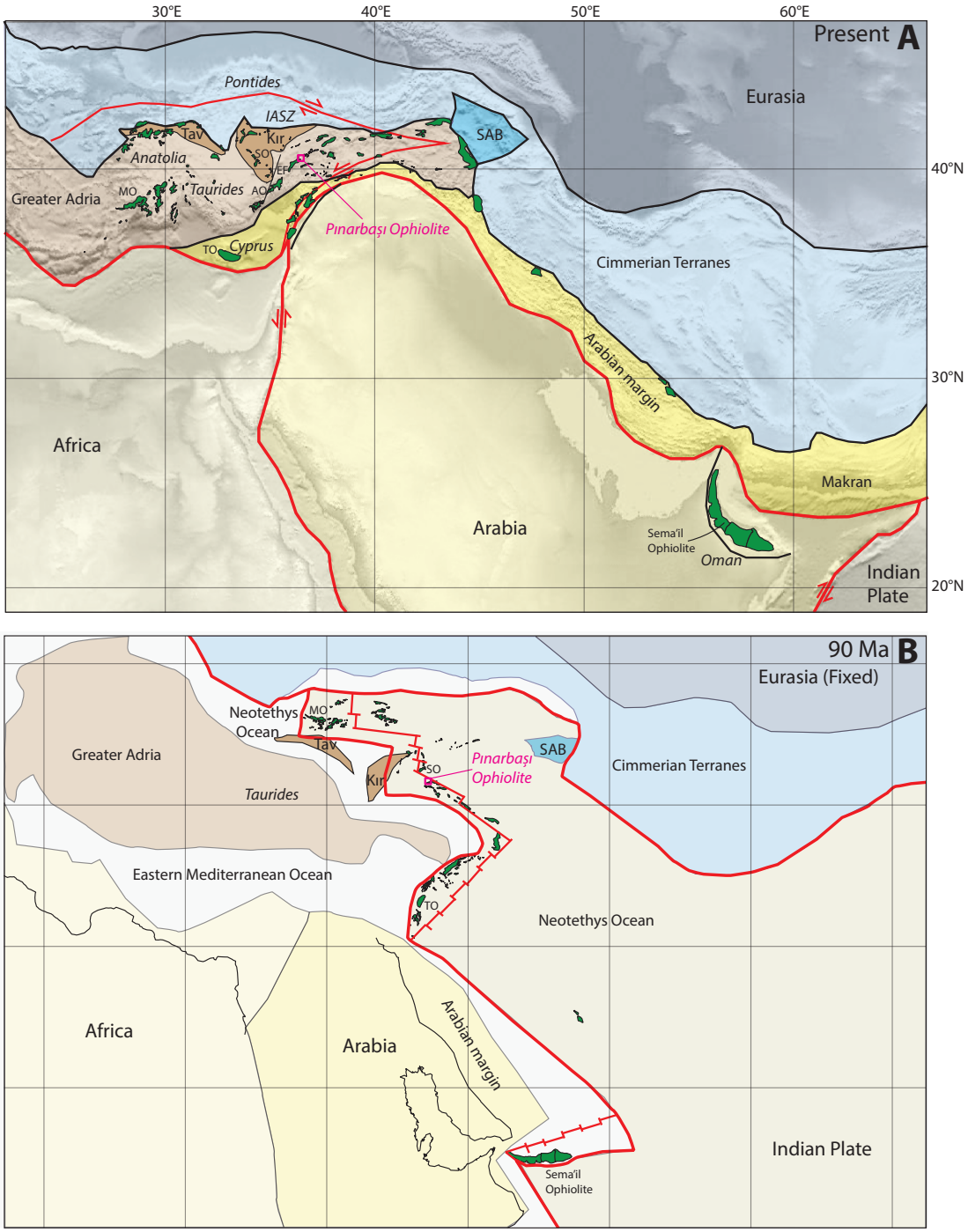


Figure 1 – (A) Tectonic map of the Alpine-Himalayan orogen between Africa, Arabia, and Eurasia, with the major ophiolite occurrences (green) that recorded Cretaceous intra-Neotethyan subduction initiation. (B) Tectonic reconstruction of the Neotethys with the configuration of the intra-Neotethyan subduction zone shortly after its formation and during supra-subduction zone spreading. Both maps are modified after *van Hinsbergen et al.* (2020, 2021). AO = Alihoca Ophiolite; EF = Ecemiş Fault; IASZ = Izmir-Ankara Suture Zone; Kır = Kırşehir Block; MO = Marmaris Ophiolite; SAB = South Armenian Block; SO = Sarıkaraman Ophiolite; Tav = Tavşanlı Zone; TO = Troodos Ophiolite.

initially started (e.g., along a continental margin, at a transform fault, at a mid-oceanic ridge, or in an arc; *Guilmette et al.*, 2023; *van Hinsbergen et al.*, 2019; *Maffione et al.*, 2015; *Plunder et al.*, 2020). Well-developed metamorphic sole sections that display the full inverted metamorphic sequence are thus key archives to study the subduction initiation process but are sparse, which, for instance, hampers discerning regional from temporal variations in metamorphic sole and subduction zone development.

East-central Turkey hosts the particularly well-preserved Cretaceous Pınarbaşı metamorphic sole (*Çörtük et al.*, 2023; *Vergili and Parlak*, 2005) (Figure 1). Although metamorphic sole rocks have been described from several ophiolites in Anatolia (e.g., *Çelik et al.*, 2006; *Daşçı et al.*, 2015; *Dilek and Whitney*, 1997; *Lytwyn and Casey*, 1995; *Parlak and Delaloye*, 1999; *Parlak et al.*, 2006; *Plunder et al.*, 2016; *Pourteau et al.*, 2019), and yielded a consistent picture of a Late Cretaceous sole cooling during SSZ ophiolite

formation (*Parlak*, 2016; *van Hinsbergen et al.*, 2016), these previously reported metamorphic sole locations are often fragmented and conceptually connected to the archetypal model. Plate tectonic reconstruction showed that the Pınarbaşı metamorphic sole formed at the same incipient subduction plate boundary system as the Oman sole (*van Hinsbergen et al.*, 2021), although much farther northwest, and in a Triassic rather than a Permian ocean basin (*van Hinsbergen et al.*, 2019, 2020). The Pınarbaşı metamorphic sole may thus serve to test the archetypal model and distinguish regional from plate boundary-wide aspects of sole formation.

In this paper, we report observations from field mapping of the sole, detailing lithological variation, metamorphic grade, and deformation fabrics from the outcrop scale to the microscale, as well as the relationship of the sole to the overlying ophiolite and underlying mélange. We aim to complement previous petrological work on the Pınarbaşı Ophiolite (*Çörtük et al.*, 2023; *Vergili and Parlak*, 2005) by quantifying the P–T conditions of formation. We provide new $^{40}Ar/^{39}Ar$ geochronology to test whether its cooling history coincides with supra-subduction zone oceanic spreading recorded in the ophiolites, a trend seen in these systems worldwide (e.g., *van Hinsbergen et al.*, 2015). We compare the sole structure, P–T conditions, and geochronological relationships between sole cooling and ophiolite spreading with those of other soles to establish whether the Pınarbaşı Ophiolite may serve as a representative natural laboratory for subduction initiation processes. Additionally, we provide plate tectonic context for sole formation using recent detailed kinematic reconstructions of eastern Mediterranean orogenesis. We critically evaluate similarities and differences between the Pınarbaşı metamorphic sole and other well-studied metamorphic sole sections elsewhere and identify opportunities for future study on the Pınarbaşı sole in light of current models and outstanding questions on sole formation, its role in the subduction initiation process in general, and in the establishment of the 1000s of km long subduction plate boundary in the Cretaceous Neotethys in particular.

2 History of thought on metamorphic soles and their role in understanding subduction initiation

In the early 1970s, metamorphic soles were first described as closely related to ophiolites (e.g., *Coleman*, 1971; *Reinhardt*, 1969; *Williams and Malpas*, 1972). Gradients in metamorphic temperature, pressure, and polyphase deformation were recognized in the field, all decreasing downward from the contact with the overlying undeformed and non-metamorphic ophiolite rocks. This inverse metamorphic gradient was first interpreted as a dynamothermal contact aureole caused by heating from the hot mantle section of the ophiolite as it was placed on top of the mafic rocks during obduction (*Williams and Smyth*, 1973).

Jamieson (1980, 1986) then showed a metamorphic profile through the St. Anthony Complex that constitutes the sole below the Cambrian Bay of Islands Ophiolite in Newfoundland, Canada. She revealed a steep thermal gradient with a sharp change in metamorphic pressure from 7–10 kbar near the peridotite contact to just 2 kbar at the base of the sole, and a variation in protoliths from gabbros through tholeiitic and alkaline basalts to sedimentary rocks. This evidence suggested that the sole formed by the underthrusting, heating, and accretion of oceanic crustal rocks underneath the mantle base of ophiolites.

A similar inverted metamorphic gradient was also observed in the Cretaceous Sema'il Ophiolite of Oman (*Lippard*, 1986). In both the Bay of Islands and Oman ophiolites, the metamorphic sole was found attached to the mantle section of the ophiolite, ranging in metamorphic grade from garnet-amphibolite to greenschist facies, while not exceeding a thickness of 500 m (*Jamieson*, 1986; *Searle and Cox*, 2002). Since their first recognition, metamorphic soles have been systematically found below other ophiolites, from the Tethyan region (*Al-Riyami et al.*, 2002; *Cluzel et al.*, 2012; *Çörtük et al.*, 2016; *Guilmette et al.*, 2008, 2009, 2018, 2023; *Liati et al.*, 2004; *Mahmood et al.*, 1995; *Nasrabady et al.*, 2011; *Parkinson*, 1998; *Plunder et al.*, 2020), the circum-Pacific region (*Keenan et al.*, 2016; *Lázaro et al.*, 2013; *Lus et al.*, 2004; *Mulcahy et al.*, 2018; *Wirth et al.*, 1993), and in orogens dating as far back as 800 Ma (*Abd El-Naby et al.*, 2000; *Fournier-Roy et al.*, 2024; *Mackay-Champion et al.*, 2024; *Mulder et al.*, 2016).

Geochemical studies from various ophiolites revealed that they mainly formed above subduction zones (*Miyashiro*, 1973). In the 1980s, such ophiolites became known as 'supra-subduction zone ophiolites' (*Casey and Dewey*, 1984; *Pearce et al.*, 1984), and in the 1990s, *Stern and Bloomer* (1992) suggested that they formed during or shortly after the inception of subduction. Confirmation of this idea came from geochronological data: *Hacker* (1994) and *Hacker et al.* (1996) showed that the $^{40}Ar/^{39}Ar$ cooling ages of the metamorphic sole of the Sema'il Ophiolite of Oman coincide with or shortly post-date the age of the crust of the overlying ophiolite. Later, extensive and detailed U/Pb dating of this ophiolite showed that the zircon crystallization ages of the sole and ophiolitic crust overlap in a narrow time window of ∼96 ± 0.5 Ma (*Rioux et al.*, 2013, 2016). As a result, soles and ophiolites became considered to be associated with catastrophic initiation of subduction, simultaneously heating the top of the incipient subducting plate and causing extension in the upper plate (*Gurnis et al.*, 2004; *Hall et al.*, 2003; *Stern*, 2004; *Stern and Bloomer*, 1992; *Stern et al.*, 2012).

Metamorphic soles pose two problems. First, the temperatures that they record are considerably higher at the associated pressures than expected for a normal oceanic lithospheric geotherm. This means that the burial of ocean floor along a simple thrust through oceanic lithosphere is not sufficient to explain

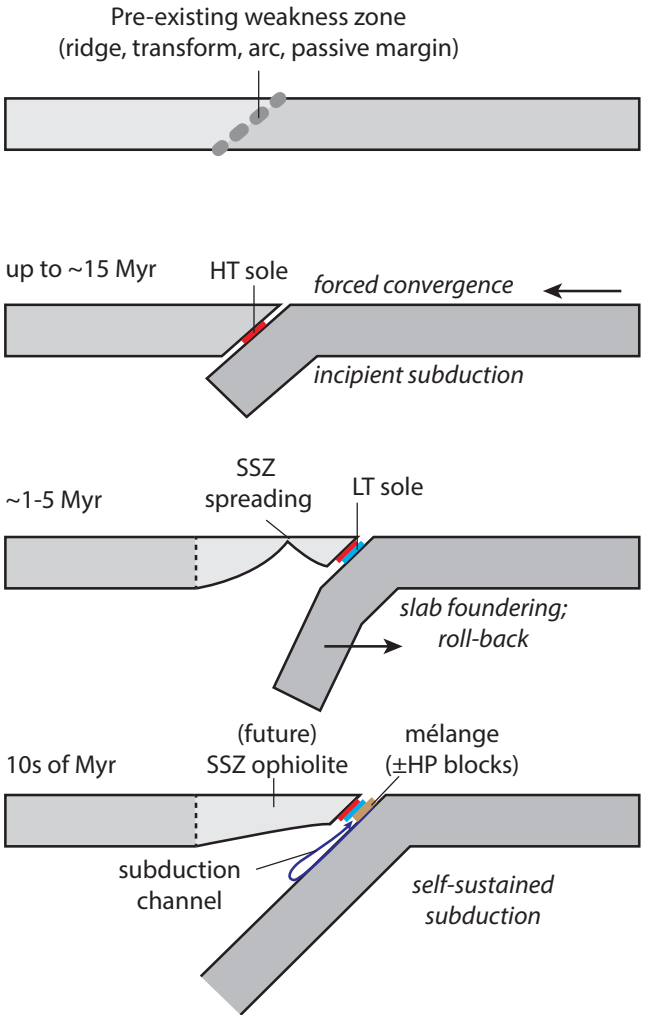


Figure 2 – Conceptual evolution of subduction initiation, metamorphic sole formation, and supra-subduction zone (SSZ) spreading. HP blocks = high-pressure metamorphic blocks. HT, LT sole = high-temperature, low-temperature sole, respectively.

the metamorphism, but a process causing additional heating is required. Second, both the recorded temperature and pressure decrease downwards showing that cooling goes hand in hand with decompression. Assuming soles and supra-subduction zone ophiolites both formed immediately after subduction initiation, explanations for the high temperatures have been sought in an anomalously hot environment during subduction initiation: by inverting mid-ocean ridges (*Duretz et al.*, 2016; *Hacker*, 1991), at off-ridge axis oceanic detachment faults (*Gülcher et al.*, 2019; *Maffione et al.*, 2015) or at transform faults between active ridges (*Dewey and Casey*, 2011; *Leng and Gurnis*, 2011). The downward-decreasing pressure has been proposed to reflect accretion of the sole during exhumation, either in a setting similar to a subduction channel (*Wakabayashi and Dilek*, 2003) or due to upper plate thinning during early subduction (*Gnos*, 1998; *Hacker and Gnos*, 1997), for instance by flattening of the plate contact (*Dewey and Casey*, 2013) due to upper plate extension and thinning (*van Hinsbergen et al.*, 2015).

The past decade saw three new additions to the understanding of metamorphic soles, shifting that perspective. First, detailed petrological mapping of soles showed that they consist of multiple, separate thrusted units that accreted from top to bottom (*Agard et al.*, 2016; *Soret et al.*, 2017). In particular, *Agard et al.* (2016) argued that the timing of accretion of these units may be associated with rheological switches, when the top contact becomes stronger than the base of the accreted units. Importantly, this showed that metamorphic soles represent a protracted period during which the plate interface undergoes net cooling. The first rock units to accrete are typically garnet amphibolites, followed by (epidote) amphibolites, at lower temperatures but not necessarily lower pressures (*Kotowski et al.*, 2021), and, finally, greenschist-facies metabasalts or metasedimentary rocks. The $^{40}Ar/^{39}Ar$ cooling ages that coincide with or shortly post-date the formation of SSZ ophiolites represent the cooling of the sole to greenschist facies conditions, i.e., coinciding with the accretion of the deepest parts of the sole. The U/Pb zircon crystallization ages, typically found in leucosomes in the sole (e.g., *Guilmette et al.*, 2018; *Rioux et al.*, 2016; *Warren et al.*, 2005) may then mark the onset of cooling of the sole below ~500 °C.

A second development came from refined geochronological analysis of the highest-grade sole parts. *Guilmette et al.* (2018) reported Lu/Hf garnet ages of ca. 104 Ma from two Sema'il localities, interpreted as garnet growth during prograde metamorphism ca. 8 Myr before bulk sole zircon and ophiolite formation at ~96 ± 0.5 Ma (*Rioux et al.*, 2013, 2016). *Garber et al.* (2020) found 107–102 Ma zircon cores coeval with those garnet ages but treated these as detrital, despite there being no known Early Cretaceous Arabian magmatism to source such grains. *Garber et al.* (2025) later reported 98 Ma Lu/Hf garnet ages and argued for a shorter lag between subduction initiation and sole cooling; alternatively, these ages may record continued garnet growth after a >100 Ma onset. *Soret et al.* (2022) support protracted metamorphism with monazite U/Pb ages of ~102–100 Ma and titanite U/Pb ages of ~100–96 Ma from the Oman sole. Thus, *Guilmette et al.* (2018), *Soret et al.* (2022), and *Garber et al.* (2025) show that sole crystallization began before ophiolite spreading. *Ring et al.* (2023, 2024) reported ~104 Ma Rb/Sr white mica ages from rocks paleogeographically linked to the Sema'il trench (*van Hinsbergen et al.*, 2019). Elsewhere, garnet Lu/Hf also predates zircon U/Pb (and amphibole $^{40}Ar/^{39}Ar$) ages, by ~15 Myr in south Tibetan soles (~145 versus ~130 Ma; *Guilmette et al.*, 2023; *Shen et al.*, 2025), and by ~10 Myr in Cordilleran sole rocks (~180 versus ~170 Ma; *Cunetta et al.*, 2025; *Mulcahy et al.*, 2018). Collectively, these data show that metamorphic soles can predate overlying ophiolitic crust by up to ~15 Myr, so subduction initiation likely begins, and may proceed slowly, well before upper plate SSZ spreading (Figure 2).

Reconstructions of the settings of subduction initiation were developed from orogenic and plate kinematic context, restoring the history after SSZ ophiolite

spreading, to infer along which structures subduction initiated. These revealed a wide variety of settings, including subduction initiation adjacent to mid-ocean ridges (Jurassic Balkan ophiolites; *Maffione et al.*, 2015; *Maffione and van Hinsbergen*, 2018), at long-lived intra-oceanic transform plate boundaries (Paleogene Marianas-Izu-Bonin subduction zone; *van de Lagemaat and van Hinsbergen*, 2024), within an arc during subduction polarity reversal (Cretaceous Andaman ophiolites; *Plunder et al.*, 2020), at ancient fracture zones in ocean floor >100 Ma old (Cretaceous Oman, Cyprus, and Anatolian ophiolites; *Maffione et al.*, 2017; *van Hinsbergen et al.*, 2021) and even at a passive continental margin (Jurassic–Early Cretaceous, southern Tibet; *Guilmette et al.*, 2023). In all cases, the metamorphic soles have nearly identical appearance, suggesting that their formation is genetically related to the processes that connect the initial thrusting to the formation of a mature subduction zone, and not to the specifics of the tectonic setting in which initial thrusting occurred (*Guilmette et al.*, 2023). This makes the study of metamorphic soles even more important to understand the subduction initiation process than previously appreciated.

3 Geological setting

Anatolia exposes an accretionary orogen that formed by subduction between the converging African and Eurasian plates since early Mesozoic time (*Şengör and Yilmaz*, 1981). The orogen contains two belts of ophiolites, one of Jurassic and one of Cretaceous age that mark two subduction systems that accommodated plate convergence (*van Hinsbergen et al.*, 2020). Both ophiolite belts have a supra-subduction zone geochemical signature and are interpreted to have formed by spreading during incipient subduction. A northern belt, with ∼170 Ma old ophiolites is located along the southern margin of the Pontide orogen that represented the southern Eurasian margin since at least mid-Mesozoic time and is interpreted to have formed in the forearc of the continent (*Çelik et al.*, 2019; *Çörtük et al.*, 2016; *Dokuz et al.*, 2017; *Şengör and Yilmaz*, 1981). These ophiolites overlie the 'Izmir-Ankara' mélange with accreted oceanic rocks of Triassic to Late Cretaceous age that is thought to represent the accretionary prism that formed during subduction of Neotethyan oceanic crust (*Sarıfakıoğlu et al.*, 2017; *Tekin et al.*, 2002; *Topuz et al.*, 2013). All supra-subduction zone ophiolites to the south of and structurally below the Izmir-Ankara mélange, including the Pınarbaşı Ophiolite that is the focus of this study, are of Cretaceous age (*Parlak*, 2016; *Robertson*, 2002; *van Hinsbergen et al.*, 2016). In Anatolia, these ophiolites form the highest structural unit above a nappe stack that was derived from Triassic ocean floor sedimentary rocks as well as slope and platform sequences derived from an adjacent microcontinental block that now form the Taurides accretionary fold-thrust belt (*McPhee et al.*, 2018a,b; *Özgül*, 1984). These continent-derived nappes accreted from Late Cretaceous to late Eocene time below the ophiolites and restore as a microcontinental terrane known as the Anatolide-Tauride platform(s) (*Şengör and Yilmaz*, 1981), which was part of the Greater Adria continental realm that stretched from the Alps and Apennines to the Iranian border (*van Hinsbergen et al.*, 2020).

However, the Cretaceous ophiolites are not restricted to the Tauride belt. They also occur to the south of the Taurides, overlying the north African margin in Cyprus, and the Arabian margin in Syria, Turkey, Iraq, Iran, and Oman (*Dilek and Furnes*, 2011; *Robertson*, 2002). Paleomagnetic evidence revealed that these ophiolites all formed by spreading above N–S striking subduction segments (*Maffione et al.*, 2017; *van Hinsbergen et al.*, 2016, 2019). Kinematic reconstruction shows that these subduction segments formed along fracture zones within the Neotethys Ocean and were connected along ∼E–W trending subduction segments that were parallel to the Greater Adria and Arabian continental margins, ending in a three-trench triple junction around the current location of northwest Anatolia (*van Hinsbergen et al.*, 2020). Paleomagnetic data from the Sema'il Ophiolite of Oman revealed similar paleo-dyke orientations and spreading directions, tracing the Cretaceous plate boundary eastwards (*van Hinsbergen et al.*, 2019), from where it connected to the Mascarene mid-oceanic ridge in the southwestern Indian Ocean and ended in a triple junction with the Southwest Indian Ridge in the southern Indian Ocean (*van Hinsbergen et al.*, 2021). Kinematic reconstruction thus suggests that the Cretaceous ophiolites of Anatolia formed at the same plate boundary as the archetypal Sema'il Ophiolite of Oman.

U/Pb zircon ages of crustal rocks of the Cretaceous ophiolites of Anatolia, NW Arabia, and Cyprus are tightly clustered between 92 and 90 Ma (*van Hinsbergen et al.*, 2016, and references therein; *Çörtük et al.*, 2025; *Parlak et al.*, 2019). In western Anatolia, kinematic reconstructions place the incipient subduction zone at which these ophiolites formed close to the continental margin. This hypothesis is supported by Greater Adria-derived detrital zircons found in the metamorphic sole of the Marmaris Ophiolite in western Turkey (*Güngör et al.*, 2019), and by the emplacement of the ophiolites onto the continental margin of the Tavşanlı Zone and Kırşehir Block of western and central Anatolia within a few million years of their crust forming by SSZ spreading (*Pourteau et al.*, 2019; *van Hinsbergen et al.*, 2016, 2025).

The ophiolites to the east of the Kırşehir Block were emplaced onto the Tauride continental margin later, from latest Cretaceous time onwards, because the Neotethyan Ocean was wider there owing to a southward step in the passive continental margin (*Gürer and van Hinsbergen*, 2019). Continued oceanic subduction below these ophiolites is reflected in the presence of gabbroic dykes intruding these ophiolites until ∼70–65 Ma (*Lytwyn and Casey*, 1995; *Parlak et al.*, 2013), showing that they remained above a mantle wedge until the latest Cretaceous. The Pınarbaşı Ophiolite also contains such Upper Cretaceous dykes (*Çörtük et al.*, 2024).

The Pınarbaşı Ophiolite is a klippe of mantle and oceanic crustal rocks in Central Anatolia, overlying the Tauride fold-and-thrust belt to the east of the Ecemiş Fault Zone that marks the eastern boundary of the Kırşehir Block (Figure 1). It overlies a metamorphic sole exposed to the south of the ophiolite (*Çörtük et al.*, 2023; *Vergili and Parlak*, 2005). Below the sole rocks is a Campanian–Maastrichtian serpentinite-matrix mélange (*Erkan et al.*, 1978). The mélange overlies the thin-skinned Taurides fold-and-thrust belt of predominantly limestone and overlying foreland basin clastic rocks of the Bolkardağ/Afyon Nappe and Geyikdağı Nappe that were underthrust below the ophiolite between the latest Cretaceous, ∼70–65 Ma, and middle Eocene time (*McPhee et al.*, 2018b; *Perincek and Kozlu*, 1984; *Pourteau et al.*, 2013; *Robertson et al.*, 2013) (Figure 1).

The ophiolite consists mostly of metasomatized mantle rocks (serpentinized peridotites, listwaenite), with pockets of pyroxenite and gabbro (*Çörtük et al.*, 2020), intruded by isolated mafic dykes (*Çörtük et al.*, 2024; *Vergili and Parlak*, 2005). These dykes have arc geochemical signatures revealing that they formed above a subduction zone and returned U/Pb zircon ages of 88.2 ± 0.4 Ma (*Çörtük et al.*, 2024) and 65.4± 3.2 Ma (*Parlak et al.*, 2013). The ophiolite does not have a well-developed crustal sequence and as a result, the age of upper plate spreading is not directly constrained. A U/Pb zircon age from gabbro in a clear crustal sequence of the Alihoca Ophiolite that lies to the west of the Ecemiş Fault is 92.4 ± 0.5 Ma (*Gürer et al.*, 2016). When the 70 km of Oligo-Miocene displacement of the Ecemiş Fault is restored (*Jaffey and Robertson*, 2001), Alihoca becomes the westward continuation of the Pınarbaşı Ophiolite (*Gürer et al.*, 2016), and its crust may thus have had the same age. However, a plagiogranite sample from the mélange below the Pınarbaşı Ophiolite returned a U/Pb zircon age of 96.8 ± 0.6 Ma, which is several million years older than any of the other known ophiolitic crustal ages (*Çörtük et al.*, 2024). The geochemistry of this plagiogranite is consistent with derivation from SSZ ophiolitic crust, but it is no longer in its original position and context. If it represents a fragment of SSZ ophiolitic crust, it shows that SSZ spreading started a few million years before the formation of the crust that is regionally preserved in the ophiolites and may have been removed by subduction erosion.

The metamorphic sole of the Pınarbaşı Ophiolite was previously described by *Çörtük et al.* (2023), who reported an inverted metamorphic sequence of, from the top, garnet amphibolites, amphibolites, and greenschists between the ophiolitic mantle section and the sub-ophiolitic mélange. Those authors performed phase equilibrium modeling on the garnet amphibolites and estimated peak P–T conditions of 1.2–1.4 GPa and 790–840 °C, in line with peak conditions in the archetypal metamorphic soles (*Jamieson*, 1986; *Searle and Cox*, 2002). Previous geochemical analyses suggested that the basaltic protoliths display a range of compositions varying from mid-ocean ridge basalt (MORB) to ocean island basalt (OIB) and island arc tholeiite (IAT) affinities (*Çörtük et al.*, 2023).

4 Field and petrographic observations

We performed detailed mapping of the metamorphic sole and obtained a large sample collection that we studied in thin section for mineralogy and microstructure. The Pınarbaşı Ophiolite is exposed west of the small village of Büyükgürleğen (Figure 3). The ophiolite forms a steeply north-dipping, lens-shaped body that extends for approximately 5 km along-strike and reaches a thickness of up to 2.5 km (Figure 3). Its pseudostratigraphy contains a crustal part (<400 m thick) in the northwest that consists of gabbro, leucocratic andesitic rocks, and hydrothermally altered mafic rocks. Structurally below this are variably serpentinized dunite and harzburgite. The peridotite is slightly foliated and crosscut by shear zones and veins that consist of pyroxenite, talc, or melt phases (feldspar). The serpentinized peridotite and the veins are cut by cm-scale brittle faults filled with serpentine. The serpentinized peridotite is also crosscut by anastomosing faults that are filled by light-colored carbonate veins. These anastomosing faults occur throughout the peridotite section of the ophiolite but become abundant close to the contact with the underlying metamorphic sole. This basal serpentinite cataclasite contains lenses of fresh and less fractured peridotite.

The metamorphic sole, found between the deformed mantle section and a chaotic, serpentinite-hosted mélange (Figure 3), is mainly composed of foliated meta-igneous and (in the lower part) meta-sedimentary rocks. The mélange has a thickness of at least 2 km and lies in thrust contact over the limestone-dominated nappes of the Taurides (Figure 3). It consists of a dominantly serpentinite matrix with greenschist, red fine-grained radiolarite, and a white to pinkish non-metamorphic sedimentary rock. The blocks in the mélange range from as small as a few centimeters up to tens of meters. The matrix is dominated by serpentinite but becomes richer in sedimentary components at lower structural levels closer to the underlying Tauride nappes. Blocks in the mélange include mantle rocks (variably serpentinized harzburgites), serpentinite cataclasite, gabbro that in some cases is overprinted by lower-amphibolite-facies metamorphism with the growth of epidote, well-foliated amphibolites that resemble those in the metamorphic sole, greenschists, slates with kink-folds, schists of which some have a purple-blue color, metapelites and calc-silicate schists, marble with chert layers of up to 10 cm, limestones, and red radiolarites.

The sole thickness is variable, due to local faulting, and reaches a maximum of 240 m (Figure 3). In its thickest, most complete section, the metamorphic grade is generally (but not everywhere, see below) inverted, with the highest-grade rocks found immediately below the peridotites. In this thickest section, we

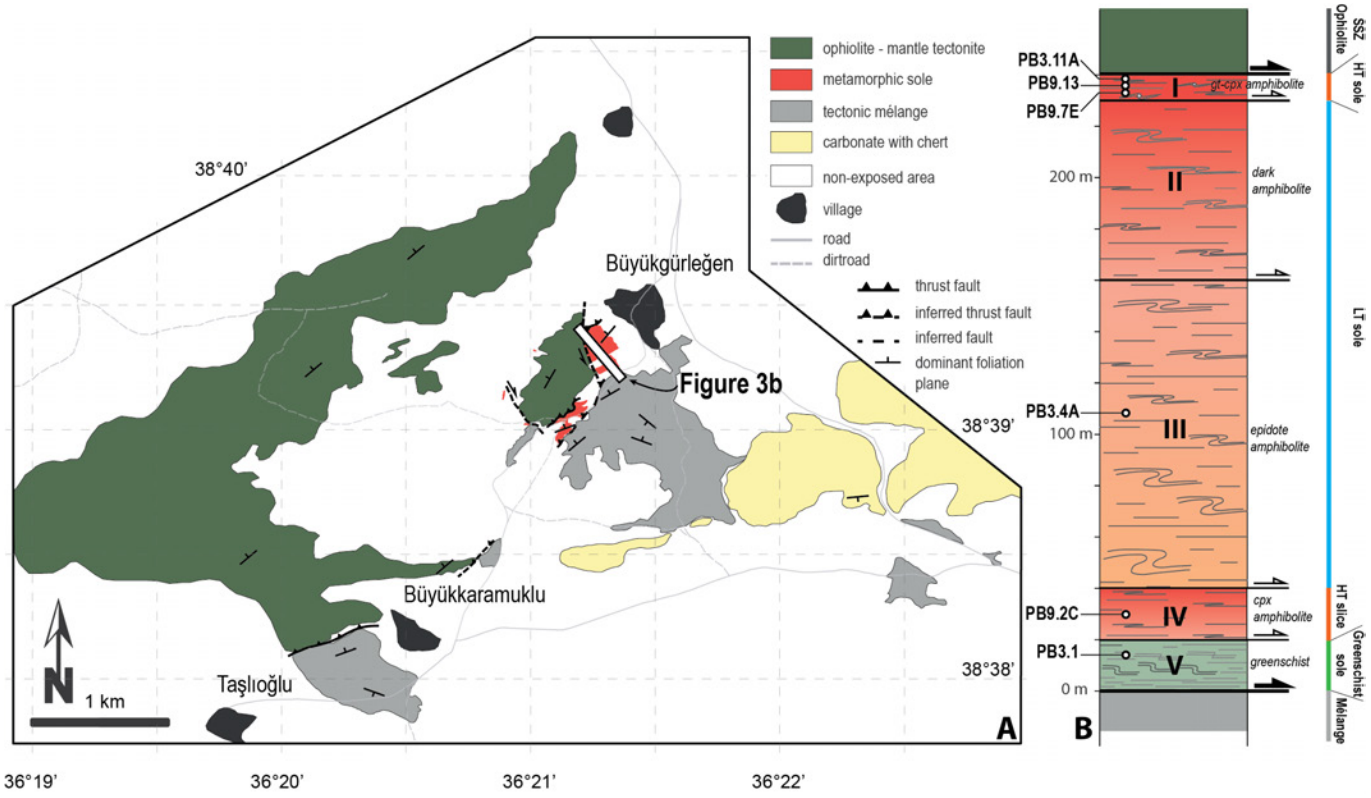


Figure 3 – (A) Geological map of the Pınarbaşı Ophiolite and underlying metamorphic sole. (B) Schematic tectono-stratigraphic log through the Pınarbaşı sole measured perpendicular to the main foliation, with the locations of the samples discussed in this paper.

made a pseudostratigraphic log (Figure 3), based on a near-continuous section sampled from gullies and exposures amidst soil, farmland, and vegetation. We identified five units based on lithology, mineral content, and structure and interpret these as the tectonostratigraphic units of the sole. From top to bottom, they consist of: (I) garnet-clinopyroxene amphibolites/granulites, with leucocratic lenses; (II) coarse-grained, black amphibolites; (III) epidote amphibolites; (IV) a slice of coarse-grained clinopyroxene amphibolite; and (V) greenschists and greenschist-facies metasedimentary rocks (Figure 4). The sole displays the general downward-decreasing metamorphic grade from garnet amphibolites to greenschist-facies rocks that is characteristic of metamorphic soles worldwide (e.g., *Dewey and Casey*, 2013; *Hacker et al.*, 1996; *Jamieson*, 1980; *Wakabayashi and Dilek*, 2003), but slice IV, with coarse-grained clinopyroxene amphibolites, breaks this trend, being of higher grade than the overlying epidote amphibolites. Below, we describe these units separately.

4.1 Unit I: Garnet-clinopyroxene amphibolites

The uppermost meter of the sole consists of dark-colored, coarse-grained, and well-foliated epidote amphibolites that are crosscut by brittle faults, likely reflecting a retrogressed zone. Below this is a garnet-clinopyroxene amphibolite unit that consists of 5 m of a relatively light-colored, weakly foliated, medium-grained garnet-clinopyroxene amphibolite. These rocks have a granoblastic texture with 1–1.5 cm lenses in which the indicator mafic minerals (clinopyroxene, amphibole, and garnet) are concentrated (Figure 4A).

Weathering surfaces typically show oxidized iron-bearing minerals. The mineral assemblage includes indicator minerals garnet, clinopyroxene, amphibole, plagioclase, quartz, titanite, and accessory phases that include apatite and zircon. The quartz crystals show undulose extinction, sub-grain formation and bulging along the grain boundaries. The foliation is defined by segregation of oriented mafic (amphibole, clinopyroxene) and felsic (plagioclase, quartz) minerals. The lineation is weakly defined by preferential orientation of hornblende. Some of the amphibole and clinopyroxene-rich layers are boudinaged, but no pressure shadows or other shear sense indicators were macroscopically observed.

Structurally below is a layer of dark-colored, well-foliated, medium-grained garnet-clinopyroxene amphibolites with a varying thickness of up to 4 m, that stands out from the higher unit by alternating lighter and darker colored bands. A clear foliation is defined by the darker bands rich in amphibole and clinopyroxene, and the lighter-colored bands rich in feldspar (Figure 4A). The garnet occurs as up to 1 cm porphyroblasts and is more abundant in the feldspar-rich bands (Figure 4A). At one location, a 3–8 cm thick layer of quartzite is observed at the upper boundary of the garnet-clinopyroxene amphibolites. The mineral assemblage in this unit consists of garnet, clinopyroxene, amphibole, plagioclase, titanite and accessory phases. The amphibole is a retrograde overprint of the garnet-clinopyroxene-plagioclase assemblage, which is

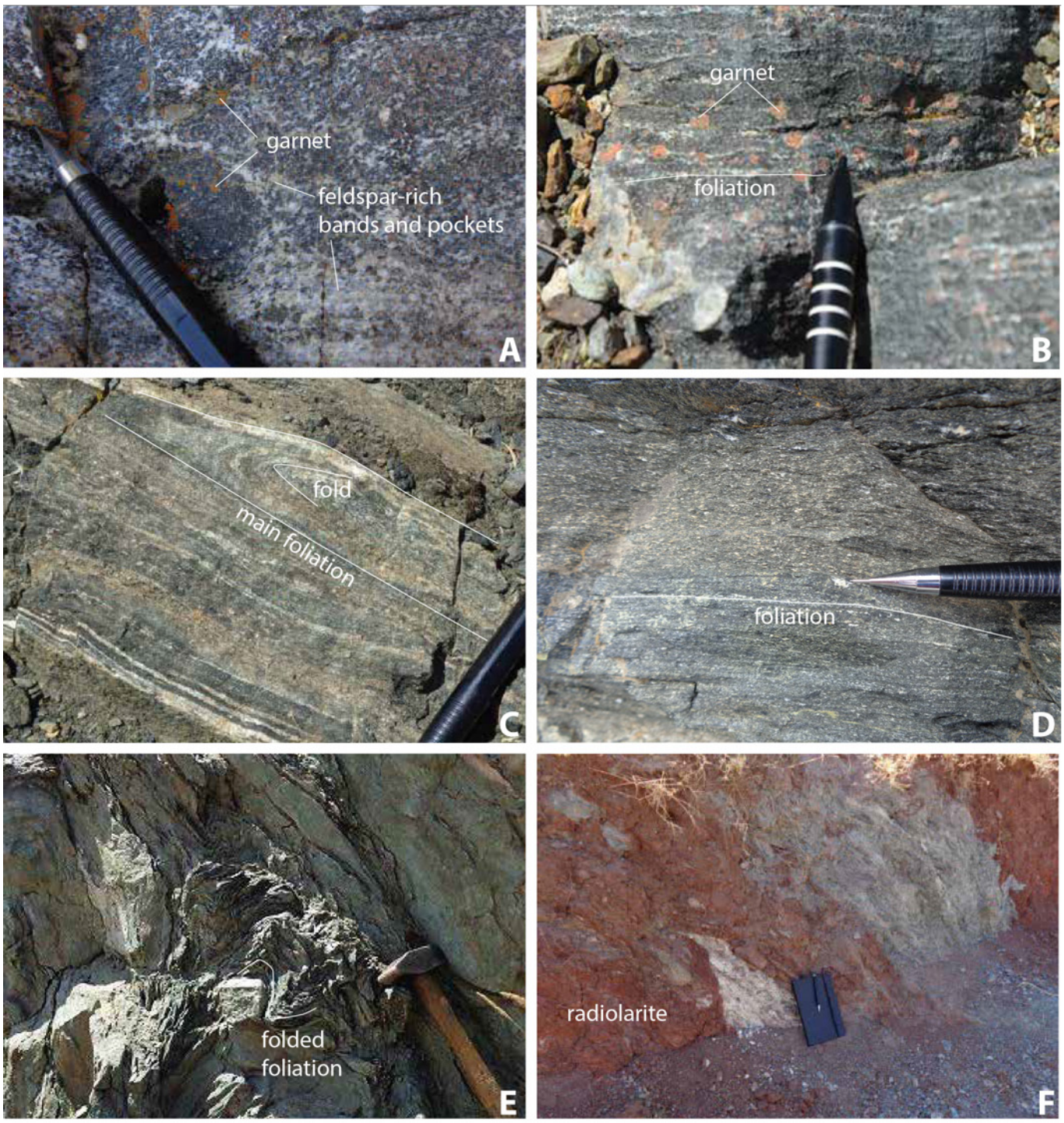


Figure 4 – Field photographs of the Pınarbaşı metamorphic sole units. (A) Garnet-clinopyroxene amphibolite with feldspar-rich pockets (Unit I); (B) garnet-clinopyroxene amphibolite (Unit I); (C) epidote amphibolite (Unit III); (D) clinopyroxene amphibolite (Unit IV); (E) greenschist (Unit V); (F) radiolarian chert in the sub-ophiolitic mélange.

still present as pockets within the amphibolite facies rock. The mineral size and abundance vary little throughout this unit. Lineations in these rocks are rare and lack asymmetric structures. Porphyroblasts line up, wrapped by the dominant foliation plane.

At thin section scale, garnet-clinopyroxene amphibolites reveal amphibole porphyroblasts of mm to cm size that occur as equidimensional to slightly elongate shapes. The amphibole and clinopyroxene porphyroblasts as well as garnets are flattened but without asymmetry. Clinopyroxene porphyroblasts contain inclusions of plagioclase, amphibole, and titanite, whereas amphibole porphyroblasts contain inclusions of plagioclase, titanite, and quartz that in turn may have inclusions of amphibole. Garnet is mm- to cm-sized, contains inclusions of quartz, clinopyroxene, amphibole, titanite and rutile and is occasionally overgrown at the rims by clinopyroxene and amphibole. In some samples (e.g., PB10.4) garnet grains are deformed and contain symmetrical pressure shadows. Millimeter- to centimeter-scale titanite crystals are aligned in the foliation plane and contain

inclusions of rutile and plagioclase. Rutile inclusions in plagioclase consist of needle-shaped crystals interpreted as having grown after titanite. The rest of the matrix consists of mm- to cm-scale plagioclase and quartz and contains, in places, small garnet grains where the assemblage is more felsic, and amphibole and minor clinopyroxene grains where more mafic.

4.2 Unit II: Coarse-grained amphibolites

Below the garnet amphibolites is an ∼80 m thick unit that consists almost exclusively of coarse-grained, black amphibolite with occasional plagioclase-rich bands. The mineral assemblage includes amphibole, plagioclase, and sub-mm titanite and rutile that also occur as inclusions in amphibole. Secondary minerals include epidote replacing plagioclase, scapolite, and zoisite, and in one sample also chlorite. This coarse-grained amphibolite unit is devoid of gradual changes in texture, mineralogy, or grain size. These amphibolites are well foliated, but a lineation is poorly developed, occasionally seen as a weak preferred orientation of hornblende crystals in the foliation plane.

4.3 Unit III: Epidote amphibolites

Below the coarse-grained amphibolite is an up to 120 m thick, well-foliated, fine-grained, epidote-rich amphibolite. This unit has a mineral assemblage composed of amphibole, epidote, plagioclase, and minor amounts of quartz, titanite, rutile and accessory phases such as apatite. Inclusions of amphibole occur in plagioclase and vice versa. Both minerals also contain rutile inclusions and apatite inclusions are found in amphibole. The main foliation plane coincides with the axial plane of isoclinal to open folds (Figure 4C). The amphibolite is compositionally banded, and the lighter bands show more randomly oriented feldspar crystals and a strong overprint by epidote.

4.4 Unit IV: Clinopyroxene amphibolites

In our section, a 20 m thick unit of coarse-grained clinopyroxene amphibolite is observed. The mineral assemblage is clinopyroxene, amphibole, plagioclase, titanite, and accessory minerals. Epidote in places overgrows amphibole. The unit is well-foliated, and the foliation is defined by amphibole and plagioclase crystals. Coarse and elongated amphibole minerals define lineations in multiple directions, with S/C fabrics showing simple shear on the scale of hand specimens.

4.5 Unit V: Greenschists

Finally, the basal 10 m of the metamorphic sole consists of well-foliated, folded and faulted greenschists. Folds are open and asymmetric and show frequent kink geometries (Figures 4E and 5). The schist consists of very fine-grained quartz, chlorite, plagioclase, very fine-grained (<10 μm) actinolite, and muscovite. Quartz and calcite veins with magnetite cut the greenschists. The foliation is defined by the micas. Ductile deformation caused (asymmetric) kink bands, followed by a fault crosscutting the dominant foliation plane. Shear bands reveal simple shear during ductile deformation.

5 P–T estimation

5.1 Methods

Electron microprobe data were acquired using a JEOL microprobe at GeoLab (Utrecht University). We adopted classical analytical conditions (15-kV acceleration voltage, 15-nA beam current, and 3-μm beam size; wavelength-dispersive spectroscopy mode). For calibration, we used albite (Si and Al), jadeite (Na), TiO_2 (Ti), adularia (K), diopside (Ca), forsterite (Mg), hematite (Fe), tephroite (Mn), and Cr_2O_3 (Cr).

All mineral formula units were calculated using an in-house MATLAB script. The calculation scheme of *Hawthorne et al.* (2012) and *Leake et al.* (1997) were used for amphibole. We selected a sample of the highest-grade rock in the sole to assess the metamorphic conditions. Sample PB9.7E is a garnet-clinopyroxene-bearing amphibolite from the structurally highest 10 m of the sole, in unit I.

We used Perple_X 7.1.13 (*Connolly*, 2009) together with the thermodynamic database of *Holland and Powell* (2011) to calculate a P–T pseudosection for sample PB9.7E. We used the set of activity–composition models as defined by *Green et al.* (2016): clinopyroxene, melt, amphibole after *Green et al.* (2016); garnet, orthopyroxene, biotite after *White et al.* (2014); ilmenite after *White et al.* (2000); feldspar after *Holland and Powell* (2011). The bulk rock composition was measured using X-ray fluorescence (XRF), corrected for apatite. The water content was conservatively taken as the loss on ignition and no oxidized iron was considered owing to the small amount of oxidation observed in the amphibole ($XFe^{3+} < 0.1$, with $XFe^{3+} = Fe^{3+} / (Fe^{3+} + Fe^{2+})$).

5.2 Results

Based on thin section observation, the peak mineral assemblage for sample PB9.7E is Grt + Cpx + Pl + Ttn / Rt + Amp + Qz (mineral abbreviations after *Whitney and Evans*, 2010). Using a thin-section scan, we estimate that the peak assemblage consists of ca. 7% garnet and 28% clinopyroxene. The rest consists of plagioclase, quartz, and amphibole as well as minor amounts of titanite (sometimes showing growth of rutile needles in its core) and rutile.

Garnet shows no zoning and has a bulk composition of $Alm_{43}Grs_{30}Prp_{23}Sps_3$ (with a standard deviation less than 0.01 for each endmember). Clinopyroxene has an average composition of diopside with an average Mg# of 0.74 (and is not shown on the P–T pseudosection for the sake of clarity). Amphibole has an average Mg# of 0.70, with almost no zoning except for retrogressed crystal rims. Plagioclase is very close to pure albite, with X_{Ab}

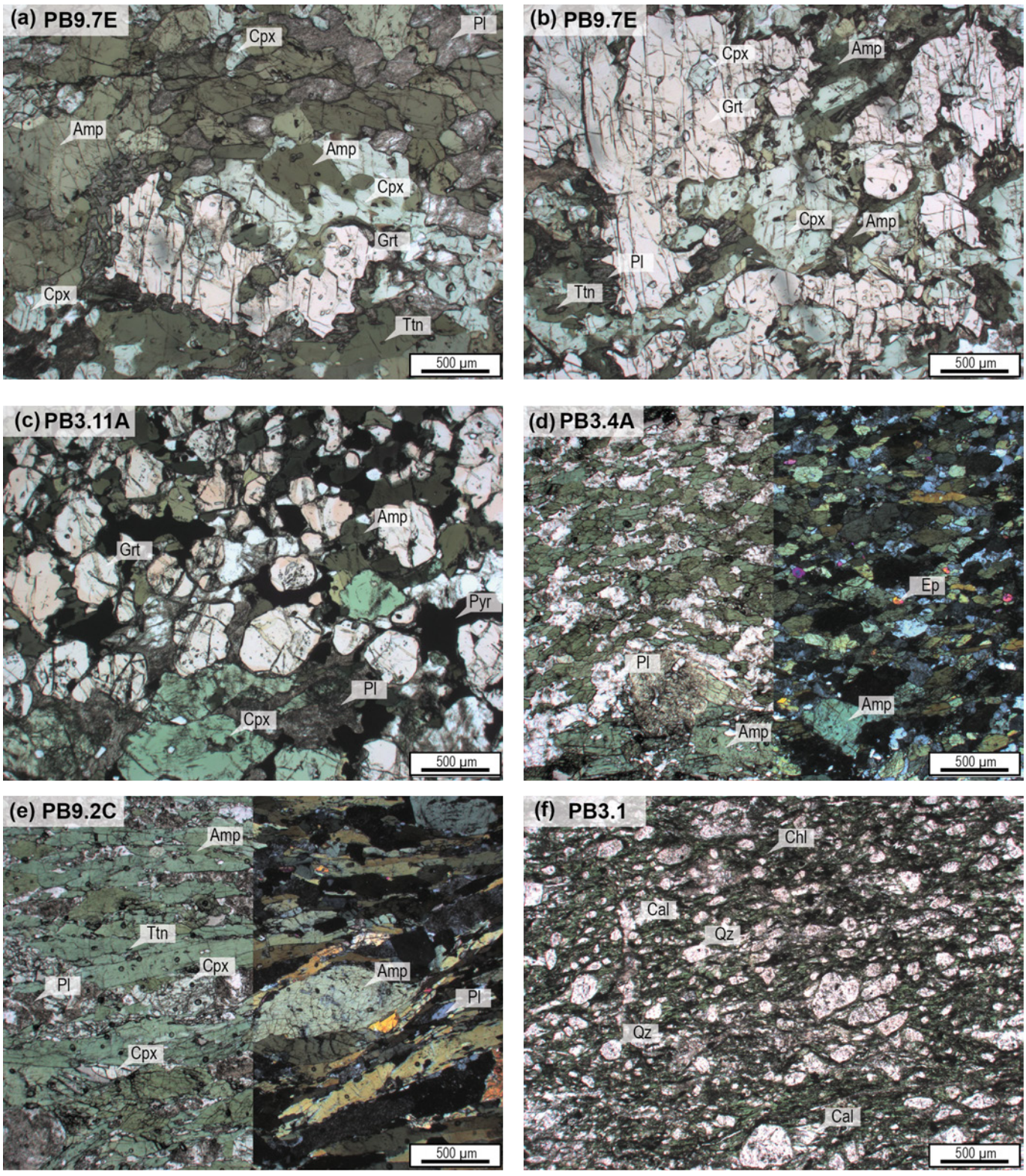


Figure 5 – (a, b) Plane-polarized light photomicrographs of sample PB9.7E. (c) Plane-polarized light photomicrograph of sample PB3.11A. (d) Plane- and cross-polarized light (left and right, respectively) photomicrograph of sample PB3.4A. (e) Plane- and cross-polarized light (left and right, respectively) photomicrograph of sample PB9.2C showing S/C' fabrics. (f) Plane-polarized light photomicrograph of sample PB3.1. Mineral abbreviations as follows: Grt, garnet; Cpx, clinopyroxene; Amp, amphibole; Pl, plagioclase; Qz, quartz; Ep, epidote; Chl, chlorite; Ttn, titanite; Pyr, pyrite; Cal, calcite.

of 0.96 on average, certainly due to strong retrogression, and could not be used for P–T determination.

Our calculated pseudosection (Figure 6) fits well with the observed mineral proportions, and the mineral compositions are similar to those measured by microprobe. The observed assemblage lies in a narrow field where titanite, rutile, and melt are stable around 800 °C and for pressures of ca. 1.0 GPa to 1.4 GPa at least. Using the composition of minerals, we further constrained the equilibration conditions of the garnet

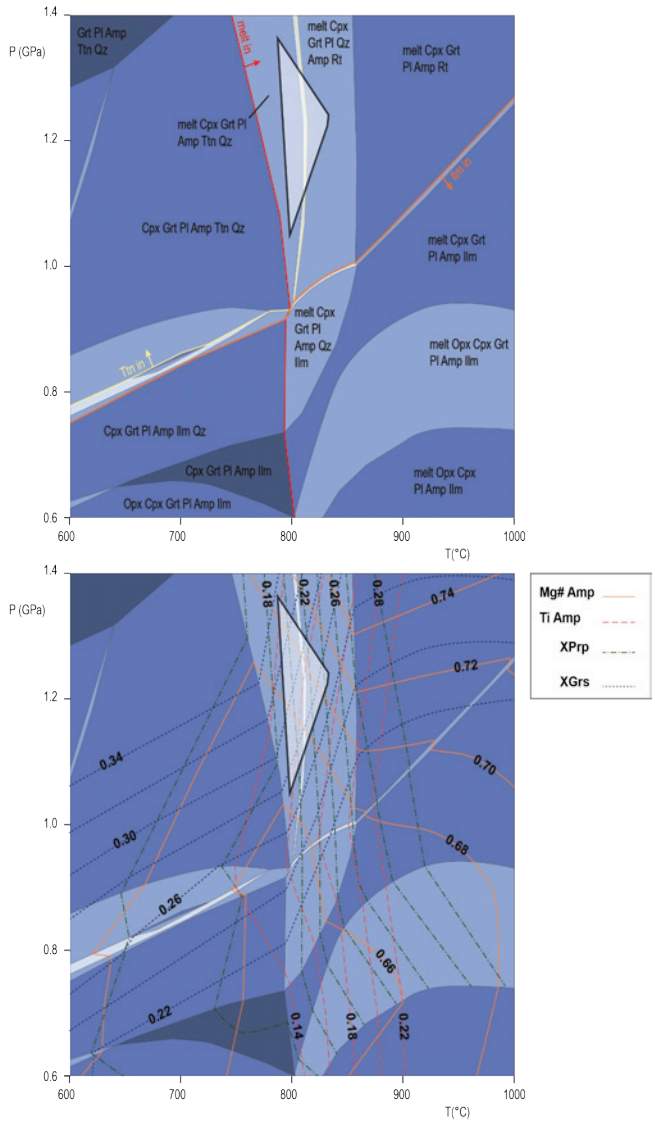


Figure 6 – P–T pseudosection for sample PB9.7E, based on a bulk-rock composition (wt%) of SiO_2 (48.576), TiO_2 (0.710), Al_2O_3 (8.709), FeO (7.702), MnO (0.147), MgO (14.169), CaO (13.562), Na_2O (2.447), H_2O (3.505). Mineral abbreviations after *Whitney and Evans* (2010).

amphibolites at the top of the sole to 1.3 ± 0.1 GPa and 800 ± 25 °C.

The calculated pressure of 1.3 GPa is slightly higher than the range of pressures obtained for other metamorphic soles in the Tauride Belt (e.g., *Dilek and Whitney*, 1997; *Plunder et al.*, 2016) but corresponds to the upper pressure estimates for metamorphic soles worldwide (e.g., *Agard et al.*, 2016). Our calculations reproduce the previous estimate of P–T conditions for the Pınarbaşı sole of *Çörtük et al.* (2023), of 1.2–1.4 GPa and 790–840 °C.

6 $^{40}Ar/^{39}Ar$ geochronology

6.1 Methods

We selected five samples for $^{40}Ar/^{39}Ar$ geochronology on amphibole. From top to bottom, we selected a garnet amphibolite with feldspar-rich pockets (PB3.11A); two samples from the garnet amphibolites without abundant pockets, namely sample PB9.7E, on which we also performed the P–T analysis above, and sample PB9.13; one epidote amphibolite (PB3.4A, unit III); and one sample from the clinopyroxene amphibolite slice (unit IV) just above the greenschist base (PB9.2C) (Figure 3).

All samples were crushed using a rock-splitter and jaw-crusher, washed and cleaned for 30 min in an ultrasonic bath. The samples were sieved in the size fraction 250–500 μm. Amphibole was concentrated using heavy liquid separations with densities of 3.1 and 3.3 g/cm^3 and Frantz magnetic separation. Final fractions were hand-picked under an optical microscope.

Samples were packaged with Drachenfels feldspar standards and were irradiated for 18 hours in the OSU Triga CLICIT facility (batch VU109). After irradiation, samples and standards were loaded in 185-hole (fusion) or 25-hole (incremental heating) Cu trays. Trays were prebaked for 24 hours under vacuum at 250 °C and subsequently placed in the sample chamber and baked at 120 °C. A 25 W Synrad CO_2 laser is used to fuse the standards and samples. The released gas is purified using the Lauda cooler at −70 °C, an NP10 at 400 °C, ST172 at 400 °C and a Ti sponge at 500 °C. The cleaned gas is expanded into a ThermoFisher Helix multi-collector mass spectrometer and ^{40}Ar is measured on the H2-Faraday cup, ^{39}Ar on the H1-Faraday or H1-compact discrete dynode secondary electron multiplier (CDD), ^{38}Ar on the AX-CDD, ^{37}Ar on the L1-CDD and ^{36}Ar on the L2-CDD.

Data reduction is performed off-line using the ArArCalc software (*Koppers*, 2002). Ages are calculated relative to an age of 25.552 ± 0.078 Ma for the Drachenfels feldspar standard based on *Wijbrans et al.* (1995) and recalibrated relative to *Kuiper et al.* (2008). Decay constants of *Min et al.* (2000) are used. The atmospheric $^{40}Ar/^{36}Ar$ ratio of 298.56 ± 0.31 is based on *Lee et al.* (2006). The correction factors and 1σ uncertainties for neutron interference reactions are (2.64 ± 0.02) × 10^{-4} for $(^{36}Ar/^{37}Ar)_{Ca}$, (6.73 ± 0.04) × 10^{-4} for $(^{39}Ar/^{37}Ar)_{Ca}$, (1.21 ± 0.003) × 10^{-2} for $(^{38}Ar/^{39}Ar)_K$ and (8.6 ± 0.7) × 10^{-4} for $(^{40}Ar/^{39}Ar)_K$. Sample analyses are corrected for gain using peak jumping of a ∼60 fA ^{40}Ar beam for all collectors and gain is calculated relative to AX-CDD. All errors are quoted at the 2σ level and include all analytical errors. All relevant analytical data for age calculations can be found in Supplementary Information 2.

6.2 Results

All data below are reported with 2σ uncertainty with their external error (including analytical error in J, but not uncertainties related to the calibration model used). This allows direct comparison of the experiments in this study. All samples have been measured twice with ^{39}Ar measured on the Faraday H1 cup in the first experiment and on the H1 CDD in the second experiment. We switched to the CDD because the ^{39}Ar beam intensity was relatively low resulting in a higher noise-to-signal

Table 1 – $^{40}Ar/^{39}Ar$ ages of the Pınarbaşı sole amphibolites. Preferred ages are highlighted in grey. Uncertainties ($\pm 2\sigma$) are given in Ma; int. = internal, ext. = external, full = including decay constant uncertainties.

		Weighted plateau								Inverse isochron							Weighted plateau with inverse isochron intercept				
Sample ID	VU ID	Age (Ma)	int. $\pm 2\sigma$	ext. $\pm 2\sigma$	full $\pm 2\sigma$	MSWD	$^{39}Ar_K$ (%)	N	N_{total}	$^{40}Ar/^{36}Ar$	$\pm 2\sigma$	Age (Ma)	int. $\pm 2\sigma$	ext. $\pm 2\sigma$	full $\pm 2\sigma$	MSWD	Age (Ma)	int. $\pm 2\sigma$	ext. $\pm 2\sigma$	full $\pm 2\sigma$	MSWD
PB9.7E	VU109-P5_1	92.50	1.45	1.45	1.56	0.78	62.9	7	11	271.1	61.0	94.41	4.46	4.46	4.5	0.71	93.58	2.46	2.46	2.53	0.33
PB9.7E	VU109-P5_2	94.52	0.40	0.41	0.71	1.79	53.8	6	12	340.4	33.9	93.03	1.24	1.25	1.37	0.49	92.96	0.64	0.64	0.86	0.19
PB9.7E	VU109-P5_2	95.22	0.89	0.90	0.98	12.85	82.9	8	12	346.1	11.2	92.92	0.60	0.61	0.71	0.85	92.89	0.24	0.25	0.45	0.48
PB9.13	VU109-P2_1	88.14	3.42	3.42	3.46	16.3	98.5	9	11	250.8	41.3	94.94	6.28	6.28	6.31	10.76	93.79	2.78	2.78	2.84	2.61
PB9.13	VU109-P2_2	94.38	0.47	0.47	0.74	1.62	98.5	15	17	301.3	8.6	94.00	1.31	1.31	1.43	1.69	93.96	0.50	0.50	0.76	0.84
PB3.11A	VU109-P1_1	93.46	0.70	0.71	0.91	1.62	31.2	5	11	347.0	74.2	89.93	5.6	5.6	5.63	1.42	89.95	2.51	2.51	2.57	0.12
PB3.11A	VU109-P1_2	94.90	0.32	0.32	0.66	1.83	60.9	12	17	309.8	65.8	94.22	3.95	3.95	3.99	2.01	94.29	1.22	1.22	1.35	0.13
PB3.4A	VU109-P3_1	92.02	0.30	0.30	0.64	1.48	94.7	9	11	317.1	75.9	91.78	1.12	1.12	1.25	1.62	91.45	0.61	0.62	0.83	0.31
PB3.4A	VU109-P3_2	93.38	0.19	0.20	0.60	1.33	94.0	12	15	285.5	29.3	93.53	0.4	0.4	0.7	1.35	93.48	0.2	0.22	0.61	0.72
PB9.2C	VU109-P4_1	93.65	0.83	0.83	1.01	1.37	24.9	6	11	292.6	109.5	93.80	2.59	2.59	2.65	1.74	94.13	1.28	1.28	1.40	0.52
PB9.2C	VU109-P4_2	95.02	0.13	0.15	0.60	1.60	91.5	15	18	316.7	35.8	94.86	0.36	0.37	0.69	1.61	94.85	0.14	0.16	0.6	0.87

ratio and larger analytical uncertainties in the first experiment for all samples.

The two incremental heating experiments of sample PB9.7E (VU109-P5; Unit Ia, HT sole) both show spectra that decrease towards higher percentages of released $^{39}Ar_K$, yielding weighted mean plateau ages of 92.50 ± 1.45 Ma (62.9% $^{39}Ar_K$) for P5_1 and 94.52 ± 0.40 Ma for P5_2 (53.8% $^{39}Ar_K$, MSWD 1.79, n = 6). Sample P5_1 has large uncertainties due to the high noise-to-signal ratio of the ^{39}Ar beam on the H1 Faraday. The age for P5_2 is more precise but shows indications of excess argon with an inverse isochron intercept ($(^{40}Ar/^{36}Ar)_0$) of 346.1 ± 11.2. In fact, the inverse isochron including 8 incremental heating steps better constrains the non-radiogenic intercept with a recalculated weighted plateau age (red age spectrum in Figure 7, continued) of 92.89 ± 0.25 Ma (Table 1).

The two incremental heating experiments of sample PB9.13 (VU109-P2; Unit I) are not reproducible. Experiment P2_1 shows alternating ages throughout the spectrum and a reliable age cannot be derived. After a few initial older steps, experiment P2_2 shows a flat age spectrum yielding 94.38 ± 0.47 Ma comprising 98.5% of the $^{39}Ar_K$ released. The $^{40}Ar/^{36}Ar$ inverse isochron intercept is 301.3 ± 8.6 and overlaps with atmospheric argon (Figure 7, Table 1).

The two incremental heating experiments of sample PB3.11A (VU109-P1; Unit I) show similar behavior with older initial steps decreasing to a plateau in the higher temperature steps. P1_1 yields 93.46 ± 0.71 Ma with 31.2% $^{39}Ar_K$ included in the plateau age and P1_2 yields 94.90 ± 0.71 Ma with 60.9% $^{39}Ar_K$. The inverse isochron intercepts are poorly constrained due to clustering of the data but do overlap with atmospheric $^{40}Ar/^{36}Ar$ (Figure 7, Table 1).

The two incremental heating experiments of sample PB3.4A (VU109-P3; Unit III, LT sole) show the same behavior, but incremental heating steps are more evenly distributed in experiment P3_2. Experiment P3_1 yields 92.02 ± 0.30 Ma ($^{39}Ar_K$ 94.7%) and P3_2 yields 93.38 ± 0.20 Ma ($^{39}Ar_K$ 94.0%). Inverse isochrons are rather clustered and intercepts do not deviate from atmospheric argon (Figure 7, Table 1).

The two incremental heating experiments of sample PB9.2C (VU109-P4; Unit IV, HT slice) yield 93.65 ± 0.83 Ma ($^{39}Ar_K$ 24.9%) for P4_1 and 95.02 ± 0.13 Ma ($^{39}Ar_K$ 91.5%) for P4_2. Inverse isochrons are rather clustered and intercepts do not deviate from atmospheric argon. P4_1 shows a decreasing spectrum with rather large uncertainties due to the high noise-to-signal ratio for ^{39}Ar when measured on the Faraday cup. In P4_2 heating steps are more evenly distributed and ^{39}Ar signal is more precisely measured on the H1-CDD. The ∼95 Ma age is therefore the preferred age (Figure 7, Table 1).

To summarize the ages from top to bottom in the metamorphic sole: the upper HT sole units I and II show ages of 92.89 ± 0.25 Ma (PB9.7E/P5), 94.38 ± 0.47 Ma (PB9.13/P2) and 94.90 ± 0.71 Ma (PB3.11A/P1), the LT sole, unit III 93.38 ± 0.20 Ma (PB3.4A/P3) and the lowermost HT slice, unit IV 95.02 ± 0.13 Ma (PB9.2C/P4). Note that full external errors including decay constant uncertainties are on the order of 0.7 Ma.

7 Discussion

7.1 Internal structure and mode of accretion of metamorphic soles

The Pınarbaşı metamorphic sole contains all elements that have widely been recognized in metamorphic soles worldwide. The top ∼10 m consists of garnet amphibolites that are widely referred to as the 'high temperature' sole (e.g., *Kotowski et al.*, 2026). We interpret the light-colored, feldspar-rich pockets in the garnet-clinopyroxene amphibolites of unit I (Figure 4A) as melt pockets. Such melt pockets are also recognized in the archetypal localities, including in the Cretaceous Sema'il soles of Oman (*Guilmette et al.*, 2018; *Hacker and Gnos*, 1997; *Searle and Malpas*, 1982; *Soret et al.*, 2019), the Cambrian Bay of Islands metamorphic soles (*Suhr and Cawood*, 1993), and elsewhere, e.g., in the Ordovician Mt. Albert sole of Canada (*Dubacq et al.*, 2019; *Kotowski et al.*, 2026; *O'Beirne-Ryan et al.*, 1990) or the Devonian

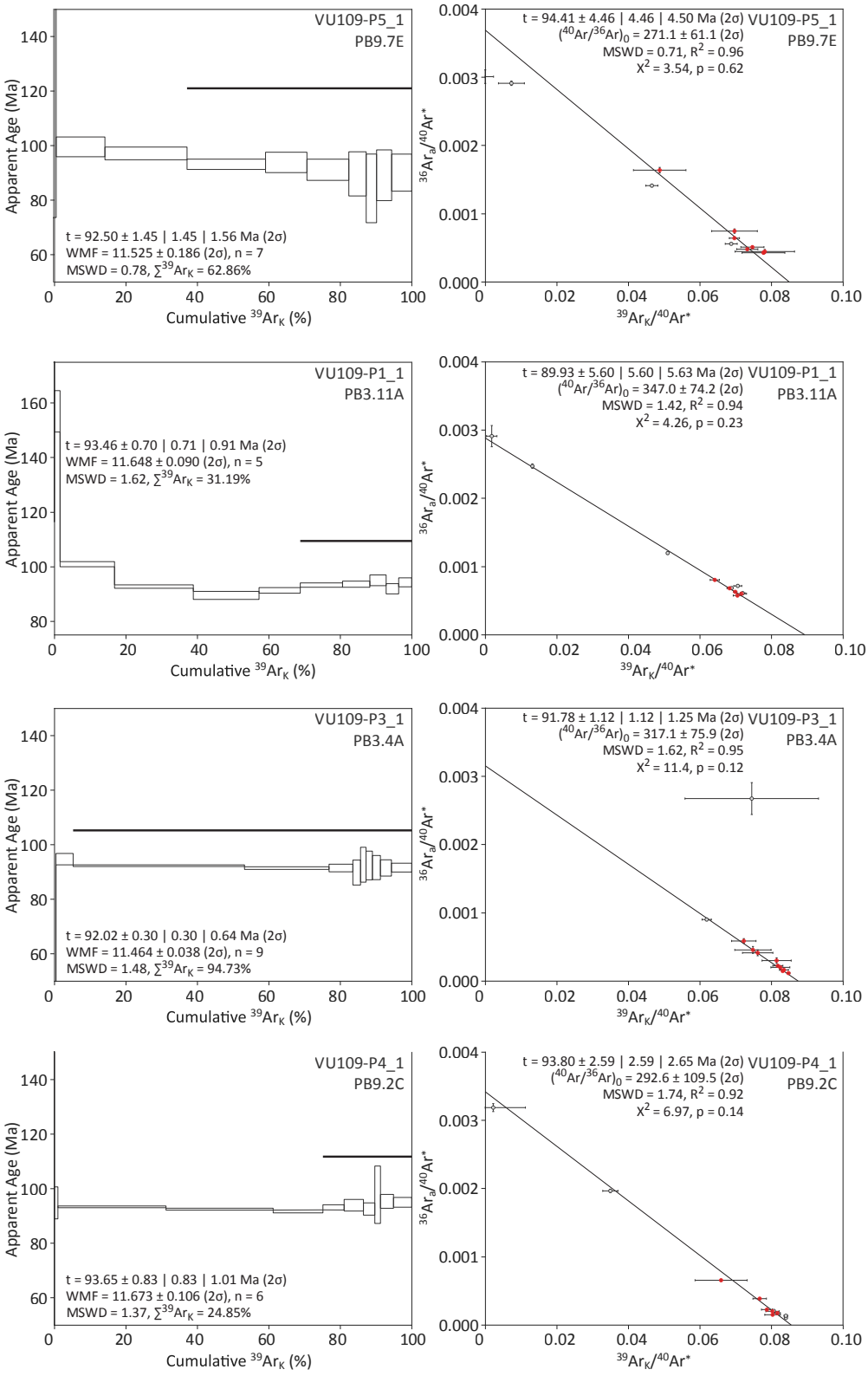


Figure 7 – $^{40}Ar/^{39}Ar$ age spectra and inverse isochron diagrams for all incremental heating experiments. Thick black lines in age spectra represent heating steps included in the weighted mean age; red dots in isochron diagrams are the same steps used to calculate inverse isochron age. The red age spectrum in experiment VU109-P5_2 is the age spectrum recalculated with the $^{40}Ar/^{36}Ar$ value derived from the inverse isochron intercept.

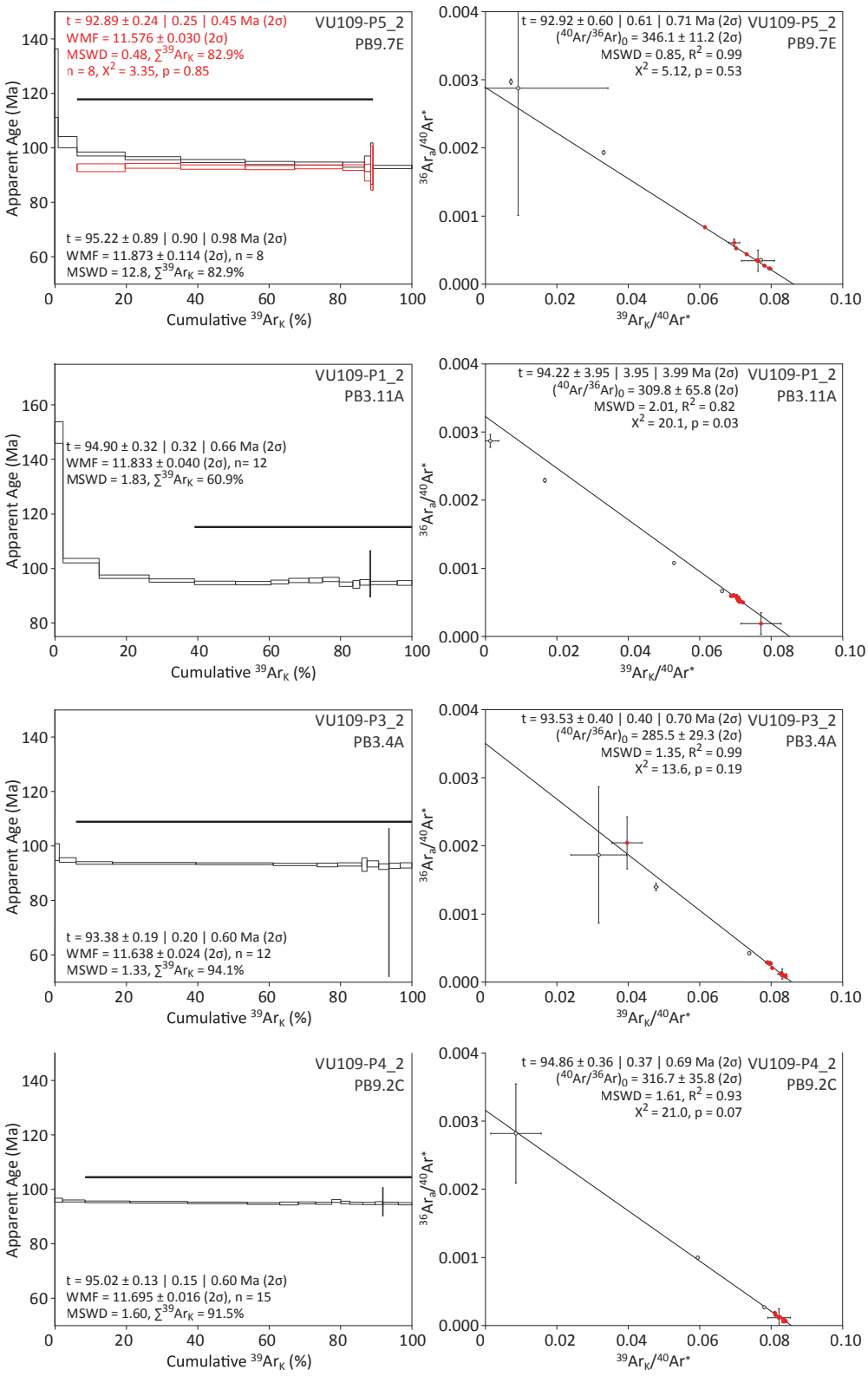


Figure 7 – (Continued).

Lizard sole of southern England (*Mackay-Champion et al.*, 2024). Structurally downwards, the sole shows a general inverted metamorphic gradient from coarse amphibolites, epidote amphibolites, to greenschists, and eventually low-grade sub-ophiolitic mélange (Figure 3), although the presence of a slice of higher-grade clinopyroxene-bearing amphibolites immediately above the greenschists at Pınarbaşı is an exception to this general trend, as discussed below.

As in other soles, metamorphic rocks with a sedimentary protolith occur only deeper in the metamorphic sole, in the greenschist-facies part of unit V (*Güngör et al.*, 2019; *Kotowski et al.*, 2021; *Myhill*, 2011). This may either suggest that accretion of seafloor rocks only occurs after the high-grade parts of the metamorphic sole formed, or that sedimentary rocks in the high-grade parts of the sole were lost to melting (*Dubacq et al.*, 2019). The former option is plausible: subduction initiated in a Triassic basin and a sedimentary cover may have been thick (e.g., *Maffione et al.*, 2017). The absence of such rocks in the top part of the sole may then suggest that this part was derived from the crustal section below the original incipient thrust that was the first to be underthrust below the ophiolite's mantle section, in which case, the early sole formed after relatively little displacement (cf. *Wakabayashi and Dilek*, 2003).

The high-grade top of the sole preserves evidence for strong flattening: pure shear appears to dominate in the HT sole, whereas simple shear seems to become more important in the LT sole. This has also been observed in other soles, such as in Oman (*Cowan et al.*, 2014; *Soret et al.*, 2019) and suggests a strong component of shear zone-perpendicular compression during HT metamorphism, and subordinate simple shear. In principle, this flattening may be well explained by the general contractional setting that is widely inferred for soles, forming at an incipient subduction plate boundary. However, this incipient subduction must contain a significant component of simple shear, and the absence of evidence for this in the HT sole of Pınarbaşı may suggest that the actual shear zone that accommodated that incipient subduction has not been preserved, because it was not accreted, or it was overprinted, or removed by later subduction erosion.

Evidence that subduction erosion may have played a role during incipient subduction and sole formation comes from the deeper part of the Pınarbaşı sole. Like other soles, the Pınarbaşı sole displays a downward-decreasing metamorphic gradient with distinct steps in metamorphic grade, which is normally interpreted as the result of episodic accretion to the metamorphic sole during plate interface cooling and exhumation (*Soret et al.*, 2017), perhaps triggered by rheological switches during gradual cooling (*Agard et al.*, 2016). The Pınarbaşı sole is thus a promising location to study the evolving rheology of nascent subduction interfaces, including the possible effects of cooling-induced changes in mineralogy (*Kotowski et al.*, 2026).

A deviation from the archetypal sole is the disruption of the downward-decreasing metamorphic grade by the slice of coarse-grained, high-temperature clinopyroxene amphibolite (unit IV). This unit is sandwiched between epidote amphibolites and greenschists in the low-temperature part of the sole. This higher-grade clinopyroxene amphibolite lens either reflects a sudden increase and then decrease in temperature during sole growth, which is unlikely given the downward-decreasing metamorphic grade observed in the Pınarbaşı sole and other soles worldwide (*Searle and Cox*, 2002; *van Hinsbergen et al.*, 2015). Alternatively, it may reflect that the lower-grade rocks above the slice were overprinted during retrogression, but we found no evidence in the field or in thin section, for instance in the form of low-grade pseudomorphs of high-grade minerals, supporting this solution. Finally, the slice may represent a structurally higher and older part of the metamorphic sole that was laterally tectonically transported along the subduction zone and re-accreted to the package that eventually formed the Pınarbaşı section. We consider the latter hypothesis more likely.

The implied tectonic repetition is interesting, because it indicates sole dismemberment. Many metamorphic soles do not contain all the elements of the pseudostratigraphy (from top to bottom, garnet-cpx amphibolites, amphibolites, epidote amphibolites, and greenschists) that is known from the type examples. Key evidence from the sole described here that suggests that metamorphic sole dismemberment occurred during sole growth includes the observation that the contact between the clinopyroxene amphibolite slice and the overlying epidote amphibolites (unit III) does not contain evidence of greenschist-facies shearing, but instead of amphibolite-facies shearing: the foliation at the top of the clinopyroxene amphibolite slice is defined by hornblende. From this, we infer that this tectonic juxtaposition occurred under amphibolite-grade conditions, prior to the accretion of the greenschist part of the sole. Moreover, the clinopyroxene amphibolite part is not underlain by epidote amphibolites, but immediately by greenschists. It thus seems to be an isolated slice that was stripped from a lower-grade underpinning, rather than a simple duplication of two laterally equivalent segments of the sole.

The tectonic repetition of high-grade metamorphic sole material may either be the result of subduction erosion, in which case it represents a fragment of exhumed HT sole closer to the trench, or of subduction channel-style exhumation, whereby it was exhumed from deeper parts of the sole. The general setting of thrusting and accretion makes the subduction erosion and re-accretion scenario more likely. Either way, the fragment may provide evidence that metamorphic soles can be imbricated during their low-temperature formation history. We are not aware of previous documentation of this phenomenon, but it may explain why soles do not always contain the full suite of facies seen in the archetypes - and that the archetypes themselves may also be incomplete.

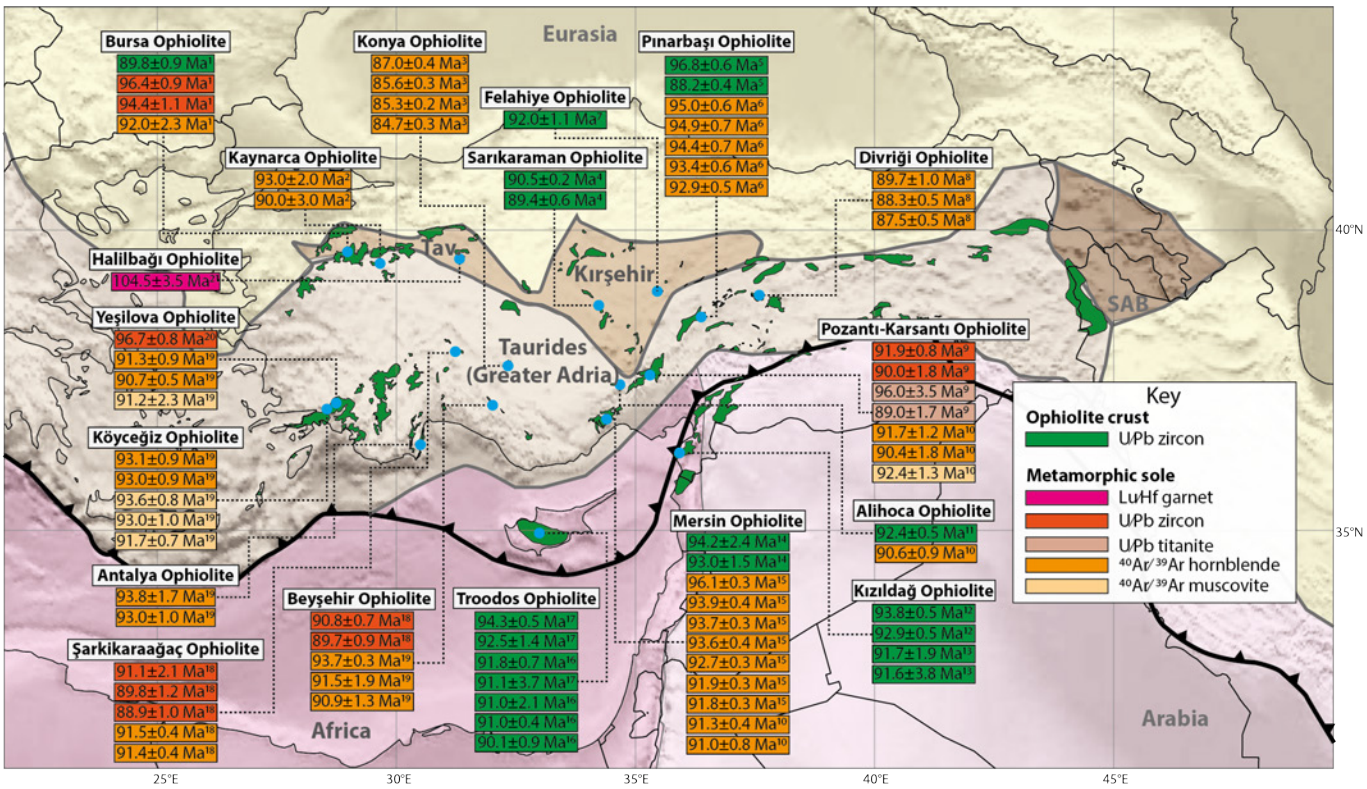


Figure 8 – Map summarizing the available age constraints on the eastern Mediterranean ophiolites and their metamorphic soles, highlighting regional differences in SSZ ophiolite spreading, sole formation and exhumation ages. SAB = South Armenian Block; Tav = Tavşanlı Zone. Key to references: 1: *Xin et al.* (2022); 2: *Önen* (2003); 3: *Daşçı et al.* (2015); 4: *van Hinsbergen et al.* (2016); 5: *Çörtük et al.* (2024); 6: this paper; 7: *Çörtük et al.* (2025); 8: *Parlak et al.* (2013); 9: *Xin et al.* (2021); 10: *Dilek et al.* (1999); 11: *Gürer et al.* (2016); 12: *Şimşek et al.* (2023); 13: *Karaoğlan et al.* (2012); 14: *Nurlu et al.* (2018); 15: *Parlak and Delaloye* (1999); 16: *Chen et al.* (2020); 17: *Morag et al.* (2020); 18: *Parlak et al.* (2019); 19: *Çelik et al.* (2006); 20: *Güngör et al.* (2019); 21: *Pourteau et al.* (2019).

7.2 Pınarbaşı sole and the regional plate tectonic context of subduction initiation

The above section highlights that the Pınarbaşı metamorphic sole contains all elements of the archetypal metamorphic soles, including the Sema'il soles of Oman and the Bay of Islands sole of Newfoundland. An added benefit of the Pınarbaşı sole is that it formed within a suite of ophiolites that are regionally extensive and well-described (e.g., *Parlak*, 2016; *Parlak et al.*, 2013; *Robertson*, 2002), that are well-dated (Figure 8), and whose tectonic setting of subduction initiation has been reconstructed in detail (*Maffione et al.*, 2017; *van Hinsbergen et al.*, 2021). This offers novel opportunities to place our new detailed field evidence in a much broader regional geodynamic context (Figure 1).

Because the climax temperatures in the amphibolites exceed the closure temperature for Ar in hornblende (~550 °C), we interpret the $^{40}Ar/^{39}Ar$ ages of the Pınarbaşı sole of ~93–95 Ma as cooling ages. They are slightly younger than the 96.8 ± 0.6 Ma U/Pb zircon age from a plagiogranite block in the Pınarbaşı mélange (*Çörtük et al.*, 2024), in line with the general trend that the $^{40}Ar/^{39}Ar$ cooling ages are similar to or slightly younger than SSZ ophiolite ages. However, the growing body of geochronological constraints on eastern Mediterranean ophiolites and soles shows some regional variation (Figure 8). We excluded from this compilation post-spreading intrusions of mafic dykes into the soles (e.g., *Parlak et al.*, 2013), and ophiolites and soles from SE Anatolia. In SE Anatolia, a geometrically complex and protracted history of back-arc basin spreading that produced oceanic crust from ~90 to 70 Ma (*van Hinsbergen et al.*, 2020) explains the much younger ages of ophiolites recorded in that region (e.g., *Bingöl et al.*, 2018; *Karaoğlan et al.*, 2012; *Nurlu*, 2020a,b, 2025; *Sapancı et al.*, 2023). For instance, U/Pb ages from a gabbro from the Alihoca Ophiolite to the southwest of Pınarbaşı gave 92.4 ± 0.5 Ma (*Gürer et al.*, 2016) and it reconstructs close to the Pınarbaşı Ophiolite when strike-slip displacement along the Oligo-Miocene Ecemiş Fault (*Jaffey and Robertson*, 2001) is restored (*Gürer and van Hinsbergen*, 2019). The Alihoca Ophiolite's metamorphic sole, moreover, generated an amphibole $^{40}Ar/^{39}Ar$ cooling age of 90.6 ± 0.9 Ma (*Dilek et al.*, 1999), somewhat younger than the cooling ages we obtained for the Pınarbaşı sole. To the northwest of the Pınarbaşı Ophiolite, plagiogranites from the Sarıkaraman Ophiolite that overlies the Kırşehir Massif gave U/Pb zircon ages as young as 90.5 ± 0.1 Ma and 89.3 ± 0.4 Ma (*van Hinsbergen et al.*, 2016). And to the west, near Konya, sole $^{40}Ar/^{39}Ar$ cooling ages are even younger, around 86 Ma (*Daşçı et al.*, 2015) (Figure 8). These ages may reflect diachronous cooling owing to differences in geodynamic evolution,

for instance due to enhanced mantle flow around the edges of narrow slab segments of the kinked intra-oceanic subduction zone above which these ophiolites formed (*Maffione et al.*, 2017). We speculate that this flow may have maintained high temperatures in the soles and caused younger cooling ages.

We believe that the ages of these Neotethyan ophiolites reflect their true spreading history. The width of the ophiolite belt, and hence the minimum width of the preserved overriding plate region is wider than in most other regions. Unlike the older ophiolites in the south and west of Anatolia, the ophiolites overlying the Kırşehir Massif do not contain metamorphic soles and restore farther away from the trench into the overriding plate (*van Hinsbergen et al.*, 2020). When post-Late Cretaceous deformation and accretion of the Anatolian orogen is restored, the Central Anatolian Ophiolites appear to have been located a few hundred kilometers away from the nearest trench. The age range of the ophiolites is straightforwardly explained by the SSZ ridge migrating away from the trench at half-spreading rate. For the Sema'il Ophiolite, half-spreading rates of 5–10 cm/yr were reconstructed from detailed U/Pb ages of sheeted dyke sections (*Rioux et al.*, 2013, 2016). Similar rates may have applied to the Anatolian ophiolites: 150–300 km of forearc crust would then have formed within a 3 Myr period, which reflects the age difference between the Alihoca and Central Anatolian Ophiolites. These younger ages show that spreading that produced the crust of the Anatolian ophiolites continued for at least several million years, and that during this upper plate spreading the formation and cooling of the metamorphic sole of Pınarbaşı, and elsewhere, continued. Anatolia may thus provide a wider former oceanic forearc region than elsewhere, from the paleo-trench in the south and west so far into the upper plate that the ophiolites towards the hinterland still contain the remains of the volcanic arc that formed upon subduction maturation (85 Ma plutons in the Kırşehir Massif; *van Hinsbergen et al.*, 2016).

8 Conclusions

In this paper, we provide comprehensive mapping and a description of the Pınarbaşı metamorphic sole in central Anatolia, as a key section to study subduction initiation dynamics. The Pınarbaşı sole is an up to 240 m thick section of meta-igneous and rare meta-sedimentary rocks below the mantle section of the supra-subduction zone Pınarbaşı Ophiolite, with an underlying serpentinite-matrix mélange. It is laterally and vertically discontinuous, showing that the sole is dismembered and the Pınarbaşı occurrence is a particularly well-preserved remnant. In its thickest section, it consists, from top to bottom, of ∼10 m of typical high-temperature sole (garnet-clinopyroxene amphibolites, in upper parts including felsic pockets interpreted as melt), and 230 m of low-temperature sole (amphibolite, epidote amphibolite, and greenschist). This inverted metamorphic gradient that is typical for soles is disrupted by a slice of clinopyroxene amphibolite that we interpret as a fragment of HT sole that was removed laterally by subduction erosion and added to the Pınarbaşı sole during LT sole formation.

For the HT sole we estimate climax P–T conditions of 1.2–1.4 GPa and 775–825 °C. From samples collected throughout the sole's pseudostratigraphy we obtained five amphibole $^{40}Ar/^{39}Ar$ cooling ages of 93–95 Ma, similar to or slightly older than regional ophiolitic crustal ages. The Cretaceous forearc ophiolites of Central Anatolia cover a paleo-forearc area with a ∼300 km across-strike breadth, much larger than Oman, and with crustal ages that may cover 3 Myr of forearc spreading, offering opportunities to study the cooling and exhumation of soles in the context of forearc extension and spreading. We conclude that the Pınarbaşı metamorphic sole provides an excellent locality to study subduction initiation dynamics from the microscale to plate boundary scale.

Acknowledgements

KP and DJJvH acknowledge funding through NWO Vidi grant 864.11.004 to DJJvH. We thank Derya Gürer, Alissa Kotowski, Lydian Boschman, and Eldert Advokaat for many discussions over the years.

Author contributions

KP: Conceptualization, Formal analysis, Investigation, Writing – original draft, Visualization
AP: Formal analysis, Investigation, Writing – review & editing, Visualization
CG: Conceptualization, *I*nvestigation, Writing – review & editing, Supervision
FMB: Formal analysis, Investigation, Writing – review & editing, Supervision
KFK: Formal analysis, Writing – original draft, Visualization
JRW: Formal analysis, Writing – review & editing
HLMvR: Investigation, Supervision
RvE: Investigation, Resources
HG: Investigation, Writing – review & editing, Visualization
JH: Investigation, Writing – review & editing, Visualization
MM: Investigation, Writing – review & editing
DJJvH: Conceptualization, Formal analysis, Resources, Investigation, Writing – original draft, Visualization, Funding acquisition, Supervision

Data availability

Supplementary Information files with microprobe analyses of sample PB9.7E, used for the pressure-temperature estimation displayed in Figure 6, and analytical details of $^{40}Ar/^{39}Ar$ data (Figure 7, Table 1) are provided through Figshare: https://doi.org/10.6084/m9.figshare.34059381.

Competing interests

The authors declare no competing interests.

Peer review

This publication was peer-reviewed by two anonymous reviewers. The full peer-review report can be found here: Review Report.

Copyright notice

© Author(s) 2026. This article is distributed under the Creative Commons Attribution 4.0 International License, which permits unrestricted use, distribution, and reproduction in any medium, provided the original author(s) and source are credited.

References

Abd El-Naby, H., W. Frisch, and E. Hegner (2000), Evolution of the Pan-African Wadi Haimur metamorphic sole, Eastern Desert, Egypt, *Journal of Metamorphic Geology*, *18*(6), 639–651, https://doi.org/10.1046/j.1525-1314.2000.00286.x.

Agard, P., P. Yamato, M. Soret, C. Prigent, S. Guillot, A. Plunder, B. Dubacq, A. Chauvet, and P. Monié (2016), Plate interface rheological switches during subduction infancy: Control on slab penetration and metamorphic sole formation, *Earth and Planetary Science Letters*, *451*, 208–220, https://doi.org/10.1016/j.epsl.2016.06.054.

Al-Riyami, K., A. Robertson, J. Dixon, and C. Xenophontos (2002), Origin and emplacement of the Late Cretaceous Baer–Bassit ophiolite and its metamorphic sole in NW Syria, *Lithos*, *65*(1–2), 225–260, https://doi.org/10.1016/s0024-4937(02)00167-6.

Bingöl, A. F., M. Beyarslan, Y.-C. Lin, and H.-Y. Lee (2018), Geochronological and geochemical constraints on the origin of the Southeast Anatolian ophiolites, Turkey, *Arabian Journal of Geosciences*, *11*(18), 569, https://doi.org/10.1007/s12517-018-3880-0.

Casey, J. F., and J. F. Dewey (1984), Initiation of subduction zones along transform and accreting plate boundaries, triple-junction evolution, and forearc spreading centres—implications for ophiolitic geology and obduction, *Geological Society, London, Special Publications*, *13*(1), 269–290, https://doi.org/10.1144/gsl.sp.1984.013.01.22.

Çelik, Ö. F., M. Delaloye, and G. Féraud (2006), Precise ^{40}Ar–^{39}Ar ages from the metamorphic sole rocks of the Tauride Belt Ophiolites, southern Turkey: implications for the rapid cooling history, *Geological Magazine*, *143*(2), 213–227, https://doi.org/10.1017/s0016756805001524.

Çelik, Ö. F., G. Topuz, Z. Billor, and M. Özkan (2019), Middle Jurassic subduction-related ophiolite fragment in Triassic accretionary complex (Mamu Dağı ophiolite, Northern Turkey), *International Geology Review*, *61*(16), 2021–2035, https://doi.org/10.1080/00206814.2019.1578109.

Chen, Y., Y. Niu, F. Shen, Y. Gao, and X. Wang (2020), New U-Pb zircon age and petrogenesis of the plagiogranite, Troodos ophiolite, Cyprus, *Lithos*, *362–363*, 105472, https://doi.org/10.1016/j.lithos.2020.105472.

Cluzel, D., F. Jourdan, S. Meffre, P. Maurizot, and S. Lesimple (2012), The metamorphic sole of New Caledonia ophiolite: ^{40}Ar/^{39}Ar, U-Pb, and geochemical evidence for subduction inception at a spreading ridge, *Tectonics*, *31*(3), TC3016, https://doi.org/10.1029/2011tc003085.

Coleman, R. G. (1971), Plate tectonic emplacement of upper mantle peridotites along continental edges, *Journal of Geophysical Research*, *76*(5), 1212–1222, https://doi.org/10.1029/jb076i005p01212.

Connolly, J. A. D. (2009), The geodynamic equation of state: what and how, *Geochemistry, Geophysics, Geosystems*, *10*(10), https://doi.org/10.1029/2009gc002540.

Çörtük, R. M., Ö. F. Çelik, M. Özkan, S. C. Sherlock, A. Marzoli, İ. E. Altıntaş, and G. Topuz (2016), Origin and geodynamic environments of the metamorphic sole rocks from the İzmir–Ankara–Erzincan suture zone (Tokat, northern Turkey), *International Geology Review*, *58*(15), 1839–1855, https://doi.org/10.1080/00206814.2016.1181991.

Çörtük, R. M., Ö. F. Çelik, A. Alkan, M. Özkan, and A. Özyavaş (2020), Distribution of rocks in Pınarbaşı Ophiolite from central Anatolia (Turkey) based on analysis of ASTER and Landsat-8 data, *Geological Journal*, *55*(10), 6810–6822, https://doi.org/10.1002/gj.3844.

Çörtük, R. M., Ö. F. Çelik, M. Özkan, A. Marzoli, and A. Alkan (2023), The origin and PT conditions of the metamorphic sole rocks beneath the Late Cretaceous Pınarbaşı Ophiolite, Eastern-Central Anatolia, *International Geology Review*, *65*(2), 296–316, https://doi.org/10.1080/00206814.2022.2045638.

Çörtük, R. M., Ö. F. Çelik, M. Özkan, J. H. F. L. Davies, and A. Marzoli (2024), Timing of the subduction initiation and ophiolite emplacement of the inner Tauride Ocean: Insight from the Pınarbaşı ophiolite in Central Türkiye, *Lithos*, *488–489*, 107833, https://doi.org/10.1016/j.lithos.2024.107833.

Çörtük, R. M., Ö. F. Çelik, M. Özkan, J. H. F. L. Davies, A. Marzoli, S. C. Sherlock, and A. M. Halton (2025), Emplacement history of the Central Anatolian Ophiolites: insights from the Felahiye Ophiolite in Central Türkiye, *International Geology Review*, *67*(9), 1251–1273, https://doi.org/10.1080/00206814.2024.2431819.

Cowan, R. J., M. P. Searle, and D. J. Waters (2014), Structure of the metamorphic sole to the Oman Ophiolite, Sumeini Window and Wadi Tayyin: implications for ophiolite obduction processes, *Geological Society, London, Special Publications*, *392*(1), 155–175, https://doi.org/10.1144/sp392.8.

Cunetta, N. S., S. R. Mulcahy, E. R. Schermer, and M. A. Smit (2025), Early Jurassic subduction initiation recorded in the Easton metamorphic suite, Northwest Cascades (Washington, USA), *Geological Society of America Bulletin*, *137*(9–10), 4431–4450, https://doi.org/10.1130/b38167.1.

Daşçı, H. T., O. Parlak, N. Nurlu, and Z. Billor (2015), Geochemical characteristics and age of metamorphic sole rocks within a Neotethyan ophiolitic mélange from Konya region (central southern Turkey), *Geodinamica Acta*, *27*(4), 223–243, https://doi.org/10.1080/09853111.2014.979532.

Dewey, J. F., and J. F. Casey (2011), The origin of obducted large-slab ophiolite complexes, in *Arc-Continent Collision*, edited by D. Brown and P. D. Ryan, pp. 431–444, Springer Berlin Heidelberg, Berlin, Heidelberg, https://doi.org/10.1007/978-3-540-88558-0_15.

Dewey, J. F., and J. F. Casey (2013), The sole of an ophiolite: the Ordovician Bay of Islands Complex, Newfoundland, *Journal of the Geological Society*, *170*(5), 715–722, https://doi.org/10.1144/jgs2013-017.

Dilek, Y., and H. Furnes (2011), Ophiolite genesis and global tectonics: Geochemical and tectonic fingerprinting of ancient oceanic lithosphere, *Geological Society of America Bulletin*, *123*(3–4), 387–411, https://doi.org/10.1130/b30446.1.

Dilek, Y., and D. L. Whitney (1997), Counterclockwise PTt trajectory from the metamorphic sole of a Neo-Tethyan ophiolite (Turkey), *Tectonophysics*, *280*(3–4), 295–310, https://doi.org/10.1016/s0040-1951(97)00038-3.

Dilek, Y., P. Thy, B. Hacker, and S. Grundvig (1999), Structure and petrology of Tauride ophiolites and mafic dike intrusions (Turkey): Implications for the Neotethyan ocean, *Geological Society of America Bulletin*, *111*(8), 1192–1216, https://doi.org/10.1130/0016-7606(1999)111<1192:sapoto>2.3.co;2.

Dokuz, A., E. Aydınçakır, R. Kandemir, O. Karslı, W. Siebel, A. S. Derman, and M. Turan (2017), Late Jurassic Magmatism and Stratigraphy in the Eastern Sakarya Zone, Turkey: Evidence for the Slab Breakoff of Paleotethyan Oceanic Lithosphere, *The Journal of Geology*, *125*(1), 1–31, https://doi.org/10.1086/689552.

Dubacq, B., M. Soret, E. Jewison, and P. Agard (2019), Early subduction dynamics recorded by the metamorphic sole of the Mt. Albert ophiolitic complex (Gaspé, Quebec), *Lithos*, *334–335*, 161–179, https://doi.org/10.1016/j.lithos.2019.03.019.

Duretz, T., P. Agard, P. Yamato, C. Ducassou, E. B. Burov, and T. V. Gerya (2016), Thermo-mechanical modeling of the obduction process based on the Oman Ophiolite case, *Gondwana Research*, *32*, 1–10, https://doi.org/10.1016/j.gr.2015.02.002.

Erkan, E., S. Özer, M. Sümengen, and I. Terlemez (1978), Sarız-Şarkışla-Gemerek-Tomarza arasının temel jeolojisi, in *Mineral Research and Exploration Institute of Turkey (MTA) Report*, vol. 5646, Mineral Research and Exploration Institute of Turkey (MTA), Ankara.

Fournier-Roy, F., C. Guilmette, K. Larson, A. Godet, M. Soret, C. van Staal, and J. H. Bédard (2024), Geochemistry and geochronology of the Bay of Islands metamorphic sole, Newfoundland, Canada: Protoliths and implications for subduction initiation, *Geological Society of America Bulletin*, *136*(1–2), 371–387, https://doi.org/10.1130/b36662.1.

Fournier-Roy, F., C. Guilmette, M. Coleman, K. Larson, D. K. Tinkham, A. M. Hinchey, J. Wakabayashi, J. H. Bédard, L. Mérit, P. Agard, L. Labrousse, and A. Godet (2026), Subduction initiation and early subduction zone development: Insights from the P–T–t path of the Bay of Islands metamorphic sole, *Journal of Metamorphic Geology*, *44*(7), 510–536, https://doi.org/10.1111/jmg.70045.

Garber, J. M., M. Rioux, A. R. C. Kylander-Clark, B. R. Hacker, J. D. Vervoort, and M. P. Searle (2020), Petrochronology of Wadi Tayin metamorphic sole metasediment, with implications for the thermal and tectonic evolution of the Samail Ophiolite (Oman/UAE), *Tectonics*, *39*(12), e2020TC006135, https://doi.org/10.1029/2020tc006135.

Garber, J. M., M. Rioux, A. J. Smye, A. M. Cruz-Uribe, P. L. Baker, J. D. Vervoort, M. P. Searle, and M. D. Feineman (2025), Shear heating during rapid subduction initiation beneath the Samail Ophiolite, *Nature Geoscience*, *18*, 653–660.

Gnos, E. (1998), Peak Metamorphic Conditions of Garnet Amphibolites Beneath the Semail Ophiolite: Implications for an Inverted Pressure Gradient, *International Geology Review*, *40*(4), 281–304, https://doi.org/10.1080/00206819809465210.

Green, E. C. R., R. W. White, J. F. A. Diener, R. Powell, T. J. B. Holland, and R. M. Palin (2016), Activity–composition relations for the calculation of partial melting equilibria in metabasic rocks, *Journal of Metamorphic Geology*, *34*(9), 845–869, https://doi.org/10.1111/jmg.12211.

Guilmette, C., R. Hébert, C. Dupuis, C. Wang, and Z. Li (2008), Metamorphic history and geodynamic significance of high-grade metabasites from the ophiolitic mélange beneath the Yarlung Zangbo ophiolites, Xigaze area, Tibet, *Journal of Asian Earth Sciences*, *32*(5–6), 423–437, https://doi.org/10.1016/j.jseaes.2007.11.013.

Guilmette, C., R. Hébert, C. Wang, and M. Villeneuve (2009), Geochemistry and geochronology of the metamorphic sole underlying the Xigaze Ophiolite, Yarlung Zangbo Suture Zone, South Tibet, *Lithos*, *112*(1–2), 149–162, https://doi.org/10.1016/j.lithos.2009.05.027.

Guilmette, C., M. A. Smit, D. J. J. van Hinsbergen, D. Gürer, F. Corfu, B. Charette, M. Maffione, O. Rabeau, and D. Savard (2018), Forced subduction initiation recorded in the sole and crust of the Semail Ophiolite of Oman, *Nature Geoscience*, *11*(9), 688–695, https://doi.org/10.1038/s41561-018-0209-2.

Guilmette, C., D. J. J. van Hinsbergen, M. A. Smit, A. Godet, F. Fournier-Roy, J. P. Butler, M. Maffione, S. Li, and K. Hodges (2023), Formation of the Xigaze Metamorphic Sole under Tibetan continental lithosphere reveals generic characteristics of subduction initiation, *Communications Earth & Environment*, *4*(1), 339, https://doi.org/10.1038/s43247-023-01007-w.

Gülcher, A. J. P., S. J. Beaussier, and T. V. Gerya (2019), On the formation of oceanic detachment faults and their influence on intra-oceanic subduction initiation: 3D thermomechanical modeling, *Earth and Planetary Science*

Letters, *506*, 195–208, https://doi.org/10.1016/j.epsl.2018.10.042.

Güngör, T., C. Akal, S. Özer, A. Hasözbek, B. Sarı, and R. Mertz-Kraus (2019), Kinematics and U-Pb zircon ages of the sole metamorphics of the Marmaris Ophiolite, Lycian Nappes, Southwest Turkey, *International Geology Review*, *61*(9), 1124–1142, https://doi.org/10.1080/00206814.2018.1498029.

Gürer, D., and D. J. J. van Hinsbergen (2019), Diachronous demise of the Neotethys Ocean as a driver for non-cylindrical orogenesis in Anatolia, *Tectonophysics*, *760*, 95–106, https://doi.org/10.1016/j.tecto.2018.06.005.

Gürer, D., D. J. J. van Hinsbergen, L. Matenco, F. Corfu, and A. Cascella (2016), Kinematics of a former oceanic plate of the Neotethys revealed by deformation in the Ulukışla basin (Turkey), *Tectonics*, *35*(10), 2385–2416, https://doi.org/10.1002/2016tc004206.

Gurnis, M., C. Hall, and L. Lavier (2004), Evolving force balance during incipient subduction, *Geochemistry, Geophysics, Geosystems*, *5*(7), https://doi.org/10.1029/2003gc000681.

Hacker, B. R. (1991), The role of deformation in the formation of metamorphic gradients: ridge subduction beneath the Oman ophiolite, *Tectonics*, *10*(2), 455–473, https://doi.org/10.1029/90tc02779.

Hacker, B. R. (1994), Rapid emplacement of young oceanic lithosphere: argon geochronology of the Oman ophiolite, *Science*, *265*(5178), 1563–1565, https://doi.org/10.1126/science.265.5178.1563.

Hacker, B. R., and E. Gnos (1997), The conundrum of Samail: explaining the metamorphic history, *Tectonophysics*, *279*(1–4), 215–226, https://doi.org/10.1016/s0040-1951(97)00114-5.

Hacker, B. R., J. L. Mosenfelder, and E. Gnos (1996), Rapid emplacement of the Oman ophiolite: Thermal and geochronologic constraints, *Tectonics*, *15*(6), 1230–1247, https://doi.org/10.1029/96tc01973.

Hall, C. E., M. Gurnis, M. Sdrolias, L. L. Lavier, and R. D. Müller (2003), Catastrophic initiation of subduction following forced convergence across fracture zones, *Earth and Planetary Science Letters*, *212*(1–2), 15–30, https://doi.org/10.1016/s0012-821x(03)00242-5.

Hawthorne, F. C., R. Oberti, G. E. Harlow, W. V. Maresch, R. F. Martin, J. C. Schumacher, and M. D. Welch (2012), Nomenclature of the amphibole supergroup, *American Mineralogist*, *97*(11–12), 2031–2048, https://doi.org/10.2138/am.2012.4276.

Holland, T. J. B., and R. Powell (2011), An improved and extended internally consistent thermodynamic dataset for phases of petrological interest, involving a new equation of state for solids, *Journal of Metamorphic Geology*, *29*(3), 333–383, https://doi.org/10.1111/j.1525-1314.2010.00923.x.

Jaffey, N., and A. H. F. Robertson (2001), New sedimentological and structural data from the Ecemiş Fault Zone, southern Turkey: implications for its timing and offset and the Cenozoic tectonic escape of Anatolia, *Journal of the Geological Society*, *158*(2), 367–378, https://doi.org/10.1144/jgs.158.2.367.

Jamieson, R. A. (1980), Formation of metamorphic aureoles beneath ophiolites—Evidence from the St. Anthony Complex, Newfoundland, *Geology*, *8*(3), 150, https://doi.org/10.1130/0091-7613(1980)8<150:forabo>2.0.co;2.

Jamieson, R. A. (1986), P-T paths from high temperature shear zones beneath ophiolites, *Journal of Metamorphic Geology*, *4*(1), 3–22.

Karaoğlan, F., O. Parlak, U. Klötzli, M. Thöni, and F. Koller (2012), U–Pb and Sm–Nd geochronology of the ophiolites from the SE Turkey: implications for the Neotethyan evolution, *Geodinamica Acta*, *25*(3–4), 146–161, https://doi.org/10.1080/09853111.2013.858948.

Keenan, T. E., J. Encarnación, R. Buchwaldt, D. Fernandez, J. Mattinson, C. Rasoazanamparany, and P. B. Luetkemeyer (2016), Rapid conversion of an oceanic spreading center to a subduction zone inferred from high-precision geochronology, *Proceedings of the National Academy of Sciences*, *113*(47), E7359–E7366, https://doi.org/10.1073/pnas.1609999113.

Koppers, A. A. P. (2002), ArArCALC—software for $^{40}Ar/^{39}Ar$ age calculations, *Computers & Geosciences*, *28*(5), 605–619, https://doi.org/10.1016/s0098-3004(01)00095-4.

Kotowski, A. J., M. Cloos, D. F. Stockli, and E. Bos Orent (2021), Structural and thermal evolution of an infant subduction shear zone: Insights from sub-ophiolite metamorphic rocks recovered from Oman Drilling Project Site BT-1B, *Journal of Geophysical Research: Solid Earth*, *126*(12), e2021JB021702, https://doi.org/10.1029/2021JB021702.

Kotowski, A. J., C. E. Seyler, J. D. Kirkpatrick, and D. J. J. van Hinsbergen (2026), Cooling-Induced Rheological Weakening Along the Nascent Plate Interface—A Mechanism for Catastrophic Subduction Initiation?, *Journal of Geophysical Research: Solid Earth*, *131*(1), e2025JB032212, https://doi.org/10.1029/2025jb032212.

Kuiper, K. F., A. Deino, F. J. Hilgen, W. Krijgsman, P. R. Renne, and J. R. Wijbrans (2008), Synchronizing rock clocks of Earth history, *Science*, *320*(5875), 500–504, https://doi.org/10.1126/science.1154339.

Lázaro, C., I. F. Blanco-Quintero, Y. Rojas-Agramonte, J. A. Proenza, K. Núñez-Cambra, and A. García-Casco (2013), First description of a metamorphic sole related to ophiolite obduction in the northern Caribbean: Geochemistry and petrology of the Güira de Jauco Amphibolite complex (eastern Cuba) and tectonic implications, *Lithos*, *179*, 193–210, https://doi.org/10.1016/j.lithos.2013.08.019.

Leake, B. E., A. R. Woolley, C. E. S. Arps, W. D. Birch, M. C. Gilbert, J. D. Grice, F. C. Hawthorne, A. Kato, H. J. Kisch, V. G. Krivovichev, K. Linthout, J. Laird, J. Mandarino, W. V. Maresch, E. H. Nickel, N. M. S. Rock, J. C. Schumacher, D. C. Smith, N. C. N. Stephenson, L. Ungaretti, E. J. W. Whittaker, and G. Youzhi (1997), Nomenclature of amphiboles: Report of the Subcommittee on Amphiboles of the International Mineralogical Association, Commission on New Minerals and Mineral Names, *The Canadian Mineralogist*, *35*(1), 219–246.

Lee, J.-Y., K. Marti, J. P. Severinghaus, K. Kawamura, H.-S. Yoo, J. B. Lee, and J. S. Kim (2006), A redetermination of the isotopic abundances of atmospheric Ar, *Geochimica et Cosmochimica Acta*, *70*(17), 4507–4512, https://doi.org/10.1016/j.gca.2006.06.1563.

Leng, W., and M. Gurnis (2011), Dynamics of subduction initiation with different evolutionary pathways, *Geochemistry, Geophysics, Geosystems*, *12*(12), Q12018, https://doi.org/10.1029/2011gc003877.

Li, Y., and M. Gurnis (2024), Rapid shear zone weakening during subduction initiation, *Proceedings of the National Academy of Sciences*, *121*(44), e2404939121.

Liati, A., D. Gebauer, and C. M. Fanning (2004), The age of ophiolitic rocks of the Hellenides (Vourinos, Pindos, Crete): first U–Pb ion microprobe (SHRIMP) zircon ages, *Chemical Geology*, *207*(3–4), 171–188, https://doi.org/10.1016/j.chemgeo.2004.02.010.

Lippard, S. J. (1986), The ophiolite of northern Oman, *Geological Society Memoir*.

Lus, W. Y., I. McDougall, and H. L. Davies (2004), Age of the metamorphic sole of the Papuan Ultramafic Belt ophiolite, Papua New Guinea, *Tectonophysics*, *392*(1–4), 85–101, https://doi.org/10.1016/j.tecto.2004.04.009.

Lytwyn, J. N., and J. F. Casey (1995), The geochemistry of postkinematic mafic dike swarms and subophiolitic metabasites, Pozanti-Karsanti ophiolite, Turkey: Evidence for ridge subduction, *Geological Society of America Bulletin*, *107*(7), 830–850, https://doi.org/10.1130/0016-7606(1995)107<0830:tgopmd>2.3.co;2.

Mackay-Champion, T. C., M. P. Searle, S. Tapster, N. M. W. Roberts, R. K. Shail, R. M. Palin, G. H. Willment, and J. T. Evans (2024), Magmatic, metamorphic and structural history of the Variscan Lizard ophiolite and metamorphic sole, Cornwall, UK, *Tectonics*, *43*(4), e2023TC008187, https://doi.org/10.1029/2023tc008187.

Maffione, M., and D. J. J. van Hinsbergen (2018), Reconstructing plate boundaries in the Jurassic Neo-Tethys from the East and West Vardar Ophiolites (Greece, Serbia), *Tectonics*, *37*(3), 858–887, https://doi.org/10.1002/2017tc004790.

Maffione, M., C. Thieulot, D. J. J. van Hinsbergen, A. Morris, O. Plümper, and W. Spakman (2015), Dynamics of intraoceanic subduction initiation: 1. Oceanic detachment fault inversion and the formation of supra-subduction zone ophiolites, *Geochemistry, Geophysics, Geosystems*, *16*(6), 1753–1770, https://doi.org/10.1002/2015gc005746.

Maffione, M., D. J. J. van Hinsbergen, G. I. N. O. de Gelder, F. C. van der Goes, and A. Morris (2017), Kinematics of Late Cretaceous subduction initiation in the Neo-Tethys Ocean reconstructed from ophiolites of Turkey, Cyprus, and Syria, *Journal of Geophysical Research: Solid Earth*, *122*(5), 3953–3976, https://doi.org/10.1002/2016jb013821.

Mahmood, K., F. Boudier, E. Gnos, P. Monié, and A. Nicolas (1995), $^{40}Ar/^{39}Ar$ dating of the emplacement of the Muslim Bagh ophiolite, Pakistan, *Tectonophysics*, *250*(1–3), 169–181, https://doi.org/10.1016/0040-1951(95)00017-5.

McPhee, P. J., D. Altıner, and D. J. J. van Hinsbergen (2018a), First Balanced Cross Section Across the Taurides Fold-Thrust Belt: Geological Constraints on the Subduction History of the Antalya Slab in Southern Anatolia, *Tectonics*, *37*(10), 3738–3759, https://doi.org/10.1029/2017TC004893.

McPhee, P. J., D. J. J. van Hinsbergen, M. Maffione, and D. Altıner (2018b), Palinspastic reconstruction versus cross-section balancing: how complete is the Central Taurides fold-thrust belt (Turkey)?, *Tectonics*, *37*(11), 4285–4310, https://doi.org/10.1029/2018tc005152.

Min, K., R. Mundil, P. R. Renne, and K. R. Ludwig (2000), A test for systematic errors in 40Ar/39Ar geochronology through comparison with U/Pb analysis of a 1.1-Ga rhyolite, *Geochimica et Cosmochimica Acta*, *64*(1), 73–98, https://doi.org/10.1016/s0016-7037(99)00204-5.

Miyashiro, A. (1973), The Troodos ophiolitic complex was probably formed in an island arc, *Earth and Planetary Science Letters*, *19*(2), 218–224, https://doi.org/10.1016/0012-821x(73)90118-0.

Morag, N., T. Golan, Y. Katzir, M. A. Coble, K. Kitajima, and J. W. Valley (2020), The origin of plagiogranites: coupled SIMS O isotope ratios, U–Pb dating and trace element composition of zircon from the Troodos Ophiolite, Cyprus, *Journal of Petrology*, *61*(5), egaa057, https://doi.org/10.1093/petrology/egaa057.

Mulcahy, S. R., J. K. Starnes, H. W. Day, M. A. Coble, and J. D. Vervoort (2018), Early onset of Franciscan subduction, *Tectonics*, *37*(5), 1194–1209, https://doi.org/10.1029/2017tc004753.

Mulder, J. A., R. F. Berry, S. Meffre, and J. A. Halpin (2016), The metamorphic sole of the western Tasmanian ophiolite: New insights into the Cambrian tectonic setting of the Gondwana Pacific margin, *Gondwana Research*, *38*, 351–369, https://doi.org/10.1016/j.gr.2015.12.010.

Myhill, R. (2011), Constraints on the evolution of the Mesohellenic Ophiolite from subophiolitic metamorphic rocks, in *Mélanges: Processes of Formation and Societal Significance*, Geological Society of America Special Papers, pp. 75–94, Geological Society of America, https://doi.org/10.1130/2011.2480(03).

Nasrabady, M., F. Rossetti, T. Theye, and G. Vignaroli (2011), Metamorphic history and geodynamic significance of the Early Cretaceous Sabzevar granulites (Sabzevar structural zone, NE Iran), *Solid Earth*, *2*(2), 219–243, https://doi.org/10.5194/se-2-219-2011.

Nurlu, N. (2020a), Geochronological, Geochemical and Sr–Nd–Pb Isotope Characteristics of the Meydan Ophiolite, SE Turkey: Petrogenesis and Implications for Mesozoic Tectonic Evolution, *Geochemistry International*, *58*(6), 639–669, https://doi.org/10.1134/s0016702920060099.

Nurlu, N. (2020b), U–Pb zircon geochronology and geochemistry of the metamorphic sole rocks of the Meydan mélange, South-East Turkey: Implications for ophiolite emplacement and protolith, *Geologica Carpathica*, *71*(2), 183–209, https://doi.org/10.31577/geolcarp.71.2.6.

Nurlu, N. (2025), New evidence on the timing of southern Neotethys closure from geochronology and geochemistry of Harmanlı region ophiolite (southeastern Anatolia) and Late Cretaceous granitic rocks, *Acta Geologica Hispanica*, *23*, 1.

Nurlu, N., S. Türkmen, G. Şimşek, and A. S. Stepanov (2018), Geochemistry and zircon U–Pb geochronology constrains late cretaceous plagiogranite intrusions in Mersin ophiolite complex (southern Turkey), *Arabian Journal of Geosciences*, *11*(23), 745, https://doi.org/10.1007/s12517-018-4120-3.

O'Beirne-Ryan, A. M., R. A. Jamieson, and Y. D. Gagnon (1990), Petrology of garnet–clinopyroxene amphibolites from Mont Albert, Gaspé, Quebec, *Canadian Journal of Earth Sciences*, *27*(1), 72–86, https://doi.org/10.1139/e90-006.

Önen, A. P. (2003), Neotethyan ophiolitic rocks of the Anatolides of NW Turkey and comparison with Tauride ophiolites, *Journal of the Geological Society*, *160*, 947–962.

Özgül, N. (1984), Stratigraphy and tectonic evolution of the Central Taurides, *Geology of the Taurus belt*, p. 77–90.

Parkinson, C. (1998), Emplacement of the East Sulawesi Ophiolite: evidence from subophiolite metamorphic rocks, *Journal of Asian Earth Sciences*, *16*(1), 13–28, https://doi.org/10.1016/s0743-9547(97)00039-1.

Parlak, O. (2016), The Tauride ophiolites of Anatolia (Turkey): A review, *Journal of Earth Science*, *27*(6), 901–934, https://doi.org/10.1007/s12583-016-0679-3.

Parlak, O., and M. Delaloye (1999), Precise $^{40}Ar/^{39}Ar$ ages from the metamorphic sole of the Mersin ophiolite (southern Turkey), *Tectonophysics*, *301*(1–2), 145–158, https://doi.org/10.1016/s0040-1951(98)00222-4.

Parlak, O., H. Yilmaz, and D. Boztuğ (2006), Origin and tectonic significance of the metamorphic sole and isolated dykes of the Divriği ophiolite (Sivas, Turkey): evidence for slab break-off prior to ophiolite emplacement, *Turkish Journal of Earth Sciences*, *15*(1), 25–45.

Parlak, O., F. Karaoğlan, T. Rızaoğlu, U. Klötzli, F. Koller, and Z. Billor (2013), U–Pb and ^{40}Ar–^{39}Ar geochronology of the ophiolites and granitoids from the Tauride belt: Implications for the evolution of the Inner Tauride suture, *Journal of Geodynamics*, *65*, 22–37, https://doi.org/10.1016/j.jog.2012.06.012.

Parlak, O., I. Dunkl, F. Karaoğlan, T. M. Kusky, C. Zhang, L. Wang, J. Koepke, Z. Billor, W. E. Hames, E. Şimşek, G. Şimşek, T. Şimşek, and S. E. Öztürk (2019), Rapid cooling history of a Neotethyan ophiolite: Evidence for contemporaneous subduction initiation and metamorphic sole formation, *Geological Society of America Bulletin*, *131*(11–12), 2011–2038, https://doi.org/10.1130/b35040.1.

Pearce, J. A., S. J. Lippard, and S. Roberts (1984), Characteristics and tectonic significance of supra-subduction zone ophiolites, *Geological Society, London, Special Publications*, *16*(1), 77–94, https://doi.org/10.1144/gsl.sp.1984.016.01.06.

Perincek, D., and H. Kozlu (1984), Stratigraphical and structural relations of the units in the Afsin-Elbistan-Doganseh ir region (Eastern Taurus), in *Geology of the Taurus Belt, Proceedings of International Symposium*, Ankara.

Plunder, A., P. Agard, C. Chopin, M. Soret, A. I. Okay, and H. Whitechurch (2016), Metamorphic sole formation, emplacement and blueschist facies overprint: early subduction dynamics witnessed by western Turkey ophiolites, *Terra Nova*, *28*(5), 329–339, https://doi.org/10.1111/ter.12225.

Plunder, A., D. Bandyopadhyay, M. Ganerød, E. L. Advokaat, B. Ghosh, P. Bandopadhyay, and D. J. J. van Hinsbergen (2020), History of subduction polarity reversal during arc-continent collision: constraints from the Andaman Ophiolite and its metamorphic sole, *Tectonics*, *39*(6), e2019TC005762, https://doi.org/10.1029/2019tc005762.

Pourteau, A., M. Sudo, O. Candan, P. Lanari, O. Vidal, and R. Oberhänsli (2013), Neotethys closure history of Anatolia: insights from ^{40}Ar–^{39}Ar geochronology and P–T estimation in high-pressure metasedimentary rocks, *Journal of Metamorphic Geology*, *31*(6), 585–606, https://doi.org/10.1111/jmg.12034.

Pourteau, A., E. E. Scherer, S. Schorn, R. Bast, A. Schmidt, and L. Ebert (2019), Thermal evolution of an ancient subduction interface revealed by Lu–Hf garnet geochronology, Halilbağı Complex (Anatolia), *Geoscience Frontiers*, *10*(1), 127–148, https://doi.org/10.1016/j.gsf.2018.03.004.

Reinhardt, B. M. (1969), On the genesis and emplacement of ophiolites in the Oman Mountains geosyncline, *Schweizer Mineralogische und Petrographische Mitteilungen*, *49*, 1.

Ring, U., J. Glodny, A. Scharf, and R. Hansman (2023), Some like it cold: The "conundrum of Samail" revisited, *Tectonics*, *42*(1), e2022TC007531, https://doi.org/10.1029/2022tc007531.

Ring, U., J. Glodny, R. Hansman, A. Scharf, F. Mattern, I. Callegari, D. J. J. van Hinsbergen, A. Willner, and Y. Hong (2024), The Samail subduction zone dilemma: Geochronology of high-pressure rocks from the Saih Hatat window, Oman, reveals juxtaposition of two subduction zones with contrasting thermal histories, *Earth-Science Reviews*, *250*, 104711, https://doi.org/10.1016/j.earscirev.2024.104711.

Rioux, M., S. Bowring, P. Kelemen, S. Gordon, R. Miller, and F. Dudás (2013), Tectonic development of the Samail ophiolite: High-precision U-Pb zircon geochronology and Sm-Nd isotopic constraints on crustal growth and emplacement, *Journal of Geophysical Research: Solid Earth*, *118*(5), 2085–2101, https://doi.org/10.1002/jgrb.50139.

Rioux, M., J. Garber, A. Bauer, S. Bowring, M. Searle, P. Kelemen, and B. Hacker (2016), Synchronous formation of the metamorphic sole and igneous crust of the Semail ophiolite: New constraints on the tectonic evolution during ophiolite formation from high-precision U–Pb zircon geochronology, *Earth and Planetary Science Letters*, *451*, 185–195, https://doi.org/10.1016/j.epsl.2016.06.051.

Robertson, A. H. F. (2002), Overview of the genesis and emplacement of Mesozoic ophiolites in the Eastern Mediterranean Tethyan region, *Lithos*, *65*(1–2), 1–67, ht

tps://doi.org/10.1016/s0024-4937(02)00160-3.

Robertson, A. H. F., O. Parlak, Y. Metin, Ö. Vergili, K. Tasli, N. İnan, and H. Soycan (2013), Late Palaeozoic–Cenozoic tectonic development of carbonate platform, margin and oceanic units in the Eastern Taurides, Turkey, *Geological Society, London, Special Publications*, *372*(1), 167–218, https://doi.org/10.1144/sp372.16.

Sapancı, Ö., G. Tokat, N. K. Eraslan, A. O. Karakaya, M. A. Gücer, and O. Çimen (2023), Geochemical and radiometric data for mafic rocks from the Guleman Ophiolite (SE, Turkey): New insights on the geodynamic evolution of the southern Neo-Tethyan ocean, *Lithos*, *442–443*, 107071, https://doi.org/10.1016/j.lithos.2023.107071.

Sarıfakıoğlu, E., Y. Dilek, and M. Sevin (2017), New synthesis of the Izmir-Ankara-Erzincan suture zone and the Ankara mélange in northern Anatolia based on new geochemical and geochronological constraints, in *Tectonic Evolution, Collision, and Seismicity of Southwest Asia: In Honor of Manuel Berberian's Forty-Five Years of Research Contributions*, *Geological Society of America Special Paper*, vol. 525, Geological Society of America.

Searle, M. P., and J. Cox (2002), Subduction zone metamorphism during formation and emplacement of the Semail ophiolite in the Oman Mountains, *Geological Magazine*, *139*(3), 241–255, https://doi.org/10.1017/s0016756802006532.

Searle, M. P., and J. Malpas (1982), Petrochemistry and origin of sub-ophiolitic metamorphic and related rocks in the Oman Mountains, *Journal of the Geological Society*, *139*(3), 235–248, https://doi.org/10.1144/gsjgs.139.3.0235.

Şengör, A. M. C., and Y. Yilmaz (1981), Tethyan evolution of Turkey: A plate tectonic approach, *Tectonophysics*, *75*(3–4), 181–241, https://doi.org/10.1016/0040-1951(81)90275-4.

Shen, J., J.-G. Dai, K. Yang, and L.-L. Zhang (2025), Protracted subduction initiation of the Neo-Tethys: Insights from metamorphic sole chronology, *Geology*, *53*(10), 803–808, https://doi.org/10.1130/g53409.1.

Shervais, J. W. (2001), Birth, death, and resurrection: The life cycle of suprasubduction zone ophiolites, *Geochemistry, Geophysics, Geosystems*, *2*(1), https://doi.org/10.1029/2000gc000080.

Şimşek, E., O. Parlak, and A. H. F. Robertson (2023), Ion-probe (SIMS) U-Pb geochronology and geochemistry of the Upper Cretaceous Kızıldağ (Hatay) ophiolite: Implications for supra-subduction zone spreading in the Southern Neotethys, *Geosystems and Geoenvironment*, *2*(3), 100165, https://doi.org/10.1016/j.geogeo.2022.100165.

Soret, M., P. Agard, B. Dubacq, A. Plunder, and P. Yamato (2017), Petrological evidence for stepwise accretion of metamorphic soles during subduction infancy (Semail ophiolite, Oman and UAE), *Journal of Metamorphic Geology*, *35*(9), 1051–1080, https://doi.org/10.1111/jmg.12267.

Soret, M., P. Agard, B. Ildefonse, B. Dubacq, C. Prigent, and C. Rosenberg (2019), Deformation mechanisms in mafic amphibolites and granulites: Record from the Semail metamorphic sole during subduction infancy, *Solid Earth*, *10*(5), 1733–1755, https://doi.org/10.5194/se-10-1733-2019.

Soret, M., G. Bonnet, P. Agard, K. P. Larson, J. M. Cottle, B. Dubacq, A. R. C. Kylander-Clark, M. Button, and N. Rividi (2022), Timescales of subduction initiation and evolution of subduction thermal regimes, *Earth and Planetary Science Letters*, *584*, 117521, https://doi.org/10.1016/j.epsl.2022.117521.

Stern, R. (2004), Subduction initiation: spontaneous and induced, *Earth and Planetary Science Letters*, *226*(3–4), 275–292, https://doi.org/10.1016/s0012-821x(04)00498-4.

Stern, R. J., and S. H. Bloomer (1992), Subduction zone infancy: Examples from the Eocene Izu-Bonin-Mariana and Jurassic California arcs, *Geological Society of America Bulletin*, *104*(12), 1621–1636, https://doi.org/10.1130/0016-7606(1992)104<1621:szieft>2.3.co;2.

Stern, R. J., and T. Gerya (2018), Subduction initiation in nature and models: A review, *Tectonophysics*, *746*, 173–198, https://doi.org/10.1016/j.tecto.2017.10.014.

Stern, R. J., M. Reagan, O. Ishizuka, Y. Ohara, and S. Whattam (2012), To understand subduction initiation, study forearc crust: To understand forearc crust, study ophiolites, *Lithosphere*, *4*(6), 469–483, https://doi.org/10.1130/l183.1.

Suhr, G., and P. A. Cawood (1993), Structural history of ophiolite obduction, Bay of Islands, Newfoundland, *Geological Society of America Bulletin*, *105*(3), 399–410, https://doi.org/10.1130/0016-7606(1993)105<0399:shooob>2.3.co;2.

Tekin, U. K., M. C. Göncüoğlu, and N. Turhan (2002), First evidence of Late Carnian radiolarians from the Izmir–Ankara suture complex, central Sakarya, Turkey: implications for the opening age of the Izmir–Ankara branch of Neo-Tethys, *Geobios*, *35*(1), 127–135, https://doi.org/10.1016/s0016-6995(02)00015-3.

Topuz, G., G. Göçmengil, Y. Rolland, Ö. F. Çelik, T. Zack, and A. K. Schmitt (2013), Jurassic accretionary complex and ophiolite from northeast Turkey: No evidence for the Cimmerian continental ribbon, *Geology*, *41*(2), 255–258, https://doi.org/10.1130/g33577.1.

van de Lagemaat, S. H. A., and D. J. J. van Hinsbergen (2024), Plate tectonic cross-roads: Reconstructing the Panthalassa-Neotethys Junction Region from Philippine Sea Plate and Australasian oceans and orogens, *Gondwana Research*, *126*, 129–201, https://doi.org/10.1016/j.gr.2023.09.013.

van Hinsbergen, D. J. J., K. Peters, M. Maffione, W. Spakman, C. Guilmette, C. Thieulot, O. Plümper, D. Gürer, F. M. Brouwer, E. Aldanmaz, and N. Kaymakcı (2015), Dynamics of intraoceanic subduction initiation: 2. Suprasubduction zone ophiolite formation and metamorphic sole exhumation in context of absolute plate motions, *Geochemistry, Geophysics, Geosystems*, *16*(6), 1771–1785, https://doi.org/10.1002/2015gc005745.

van Hinsbergen, D. J. J., M. Maffione, A. Plunder, N. Kaymakcı, M. Ganerød, B. W. H. Hendriks, F. Corfu,

D. Gürer, G. I. N. O. de Gelder, K. Peters, P. J. McPhee, F. M. Brouwer, E. L. Advokaat, and R. L. M. Vissers (2016), Tectonic evolution and paleogeography of the Kırşehir Block and the Central Anatolian Ophiolites, Turkey, *Tectonics*, *35*(4), 983–1014, https://doi.org/10.1002/2015tc004018.

van Hinsbergen, D. J. J., M. Maffione, L. M. T. Koornneef, and C. Guilmette (2019), Kinematic and paleomagnetic restoration of the Semail ophiolite (Oman) reveals subduction initiation along an ancient Neotethyan fracture zone, *Earth and Planetary Science Letters*, *518*, 183–196, https://doi.org/10.1016/j.epsl.2019.04.038.

van Hinsbergen, D. J. J., T. H. Torsvik, S. M. Schmid, L. C. Maţenco, M. Maffione, R. L. M. Vissers, D. Gürer, and W. Spakman (2020), Orogenic architecture of the Mediterranean region and kinematic reconstruction of its tectonic evolution since the Triassic, *Gondwana Research*, *81*, 79–229, https://doi.org/10.1016/j.gr.2019.07.009.

van Hinsbergen, D. J. J., B. Steinberger, C. Guilmette, M. Maffione, D. Gürer, K. Peters, A. Plunder, P. J. McPhee, C. Gaina, E. L. Advokaat, R. L. M. Vissers, and W. Spakman (2021), A record of plume-induced plate rotation triggering subduction initiation, *Nature Geoscience*, *14*(8), 626–630, https://doi.org/10.1038/s41561-021-00780-7.

van Hinsbergen, D. J. J., T. N. Lamont, and C. Guilmette (2025), Lithospheric unzipping explaining hot orogenesis during continental subduction, *Tectonics*, *44*(7), e2025TC008993, https://doi.org/10.1029/2025tc008993.

Vergili, Ö., and O. Parlak (2005), Geochemistry and tectonic setting of metamorphic sole rocks and mafic dikes from the Pinarbasi (Kayseri) Ophiolite, central Anatolia (Turkey), *Ofioliti*, *30*, 37–52, https://doi.org/10.4454/OFIOLITI.V30I1.239.

Wakabayashi, J., and Y. Dilek (2003), What constitutes 'emplacement' of an ophiolite?: Mechanisms and relationship to subduction initiation and formation of metamorphic soles, *Geological Society, London, Special Publications*, *218*(1), 427–447, https://doi.org/10.1144/gsl.sp.2003.218.01.22.

Warren, C. J., R. R. Parrish, D. J. Waters, and M. P. Searle (2005), Dating the geologic history of Oman's Semail ophiolite: Insights from U-Pb geochronology, *Contributions to Mineralogy and Petrology*, *150*(4), 403–422, https://doi.org/10.1007/s00410-005-0028-5.

White, R. W., R. Powell, T. J. B. Holland, and B. A. Worley (2000), The effect of TiO_2 and Fe_2O_3 on metapelitic assemblages at greenschist and amphibolite facies conditions: mineral equilibria calculations in the system K_2O–FeO–MgO–Al_2O_3–SiO_2–H_2O–TiO_2–Fe_2O_3, *Journal of Metamorphic Geology*, *18*(5), 497–511, https://doi.org/10.1046/j.1525-1314.2000.00269.x.

White, R. W., R. Powell, T. J. B. Holland, T. E. Johnson, and E. C. R. Green (2014), New mineral activity–composition relations for thermodynamic calculations in metapelitic systems, *Journal of Metamorphic Geology*, *32*(3), 261–286, https://doi.org/10.1111/jmg.12071.

Whitney, D. L., and B. W. Evans (2010), Abbreviations for names of rock-forming minerals, *American Mineralogist*, *95*(1), 185–187, https://doi.org/10.2138/am.2010.3371.

Wijbrans, J., M. Pringle, A. Koppers, and R. Scheveers (1995), Argon geochronology of small samples using the Vulkaan argon laserprobe, *Proceedings of the Royal Netherlands Academy of Arts and Sciences*, *98*(2), 185–218.

Williams, H., and J. Malpas (1972), Sheeted dikes and brecciated dike rocks within transported igneous complexes Bay of Islands, Western Newfoundland, *Canadian Journal of Earth Sciences*, *9*(9), 1216–1229, https://doi.org/10.1139/e72-105.

Williams, H., and W. R. Smyth (1973), Metamorphic aureoles beneath ophiolite suites and alpine peridotites; tectonic implications with west Newfoundland examples, *American Journal of Science*, *273*(7), 594–621, https://doi.org/10.2475/ajs.273.7.594.

Wirth, K. R., J. M. Bird, A. E. Blythe, D. J. Harding, and M. T. Heizler (1993), Age and evolution of western Brooks Range ophiolites, Alaska: Results from $^{40}Ar/^{39}Ar$ thermochronometry, *Tectonics*, *12*(2), 410–432, https://doi.org/10.1029/92tc02640.

Xin, G.-Y., Y. Chu, B.-X. Su, W. Lin, I. Uysal, and Z.-T. Feng (2021), Rapid transition from MORB-type to SSZ-type oceanic crust generation following subduction initiation: insights from the mafic dikes and metamorphic soles in the Pozantı-Karsantı ophiolite, SE Turkey, *Contributions to Mineralogy and Petrology*, *176*(9), 64, https://doi.org/10.1007/s00410-021-01821-5.

Xin, G.-Y., Y. Chu, B.-X. Su, W. Lin, M.-M. Cui, X. Liu, I. Uysal, J.-L. Li, and Z.-T. Feng (2022), Subduction initiation in the Neo-Tethys and formation of the Bursa ophiolite in NW Turkey, *Lithos*, *422–423*, 106746, https://doi.org/10.1016/j.lithos.2022.106746.